

Submitted to Journal of Chemical Physics

LBL-6976
Preprint c. 2

RECEIVED
LAWRENCE
BERKELEY LABORATORY

JAN 27 1978

LIBRARY AND
DOCUMENTS SECTION

DEUTERIUM MAGNETIC RESONANCE OF SOME
POLYMORPHIC LIQUID CRYSTALS: THE
CONFORMATION OF THE ALIPHATIC END CHAINS

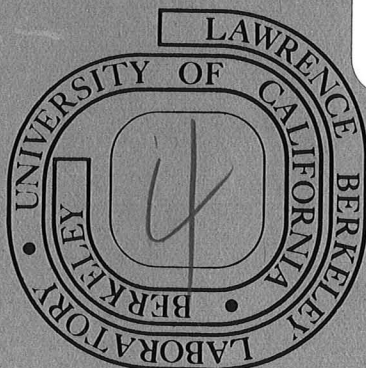
Shan Hsi, Herbert Zimmermann, and
Zeev Luz

October 1977

Prepared for the U. S. Department of Energy
under Contract W-7405-ENG-48

TWO-WEEK LOAN COPY

*This is a Library Circulating Copy
which may be borrowed for two weeks.
For a personal retention copy, call
Tech. Info. Division, Ext. 5716*



LBL-6976
c. 2

— LEGAL NOTICE —

This report was prepared as an account of work sponsored by the United States Government. Neither the United States nor the Department of Energy, nor any of their employees, nor any of their contractors, subcontractors, or their employees, makes any warranty, express or implied, or assumes any legal liability or responsibility for the accuracy, completeness or usefulness of any information, apparatus, product or process disclosed, or represents that its use would not infringe privately owned rights.

DEUTERIUM MAGNETIC RESONANCE OF SOME
POLYMORPHIC LIQUID CRYSTALS: THE CONFORMATION
OF THE ALIPHATIC END CHAINS*

By

Shan Hsi, Herbert Zimmermann,
and Zeev Luz[†]

Department of Chemistry, Materials and Molecular Research Division,
Lawrence Berkeley Laboratory, University of California
Berkeley, California 94720

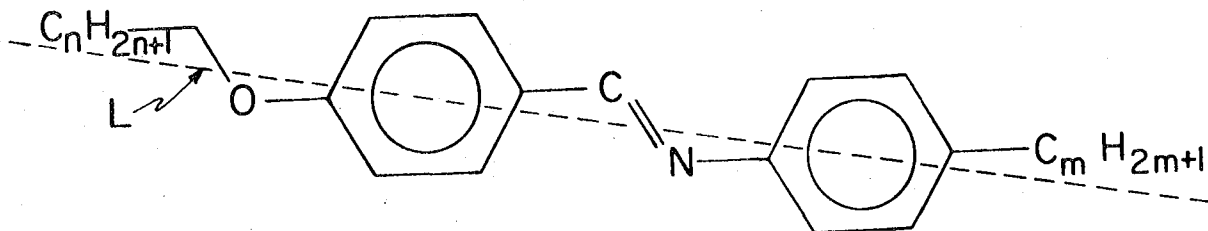
ABSTRACT

Deuterium magnetic resonance measurements of four members of the homologous series p-alkoxybenzylidene-p-alkylaniline($n \cdot m$), perdeuterated in their alkoxy chains, are reported. The compounds studied were 40·7, 50·7, 60·7 and 70·7. For 50·7 various isotopic species specifically deuterated in the alkoxy chains, as well as in the benzylidene moiety, were prepared and their DMR studied. These measurements allowed a complete assignment of the resonances from the alkoxy chain. The spectrum of all four compounds was studied over their whole mesomorphic regions. In most phases well resolved spectra were obtained yielding the various quadrupole splittings and in many cases also the dipolar interactions within the methylene and methyl groups. Using double quantum spectroscopy dipolar splitting between different methylene deuterons could also be resolved. The methylene quadrupolar splittings and the dipolar interaction within the methylene groups decrease along the chain towards the methyl end in a characteristic stepwise manner. This behavior is attributed to chain reorientational freedom and is quantitatively interpreted in terms of two structural factors: (i) Fast dynamical equilibrium between the all-trans conformation of the alkoxy chains and chain conformations involving one or more kinks, and (ii) A molecular model in which the aliphatic chain axis is inclined with respect to the molecular long axis. The characteristic pattern of the splitting can then be reproduced by assuming a monotonically increasing kink probabilities along the chain towards its methyl end. This interpretation is used to estimate the kink probability distribution in the alkoxy chains in the various compounds and mesophases. No significant effect of the mesophase structure on the kink statistics was found.

I. INTRODUCTION

Nuclear magnetic resonance spectroscopy has been used extensively to study molecular structure and ordering of liquid crystalline phases. The earlier workers^{1,2} used proton magnetic resonance, but this spectroscopy is hampered by the complexity of the spectrum caused by excessive number of protons per molecule and the large dipolar interaction between them.¹⁻⁶ The NMR spectrum may sometimes be simplified by using other nuclei such as ¹⁹F in fluorinated liquid crystals,⁷ or ¹³C using enhancement techniques.^{8,9} Particularly useful is deuterium magnetic resonance¹⁰ of deuterated compounds. The first application of this technique was made by Rowell et al.¹¹ in 1965 on the nematic phase of a number of liquid crystals. More recently this approach has been extended and used to study molecular ordering in a wide variety of thermotropic¹²⁻¹⁹ and lyotropic²⁰⁻³⁵ mesophases. An extensive review on deuterium NMR including an essentially complete literature coverage of the liquid crystal work was recently published.³⁶

In the present paper we report a deuterium magnetic resonance study on four members of the homologous series, p-alkoxybenzylidene-p-alkylaniline ($C_n H_{2n+1} OC_6 H_4 CHNC_6 H_4 C_m H_{2m+1}$) commonly referred to as no•m. The compounds studied were 40•7, 50•7, 60•7 and 70•7.



The higher members of this series are polymorphic and exhibit a number of different mesomorphic phases.³⁷⁻⁴² The compounds studied were deuterated in their alkoxy chains, and we attempted to use their deuterium resonance in order to study the conformation equilibria of the chains, and determine whether any correlation existed between the chain conformation and the structure of the mesophases.

The thermodynamic properties of this homologous series were studied previously by calorimetric methods and some of the mesophase's structures were determined by optical microscopy and X-ray techniques.³⁷⁻⁴² The phase diagrams for the four compounds studied in the present work are given in Table I. The assignment of the smectic phases in 50·7 and 70·7 were established by X-ray spectroscopy.⁴¹ (In 40·7 we found both by microscopy as well as by the NMR behavior of the spectrum an extra phase over a narrow temperature range between the smectic A and B phases, which by analogy with the other members of the series we tentatively identified as smectic C.) It may be seen in Table I that the transition temperatures for the deuterated compounds are lower (in the case of 70·7 by more than ten degrees) relative to the literature values. In part, this is due to deuterium isotope effect on the phase transition temperature, but it may also be due to the presence of impurities.

Using a superconducting high field magnet and fast Fourier Transform techniques we obtained high quality spectra in which the various methylene (and methyl) resonances were often well resolved. The NMR techniques and the synthesis of the deuterated compounds are described in Section II. For one compound (50·7) we made an unambiguous peak assignment using various

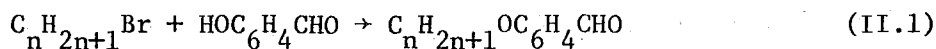
isotopically substituted compounds. This analysis is described in Section III. In most phases the resolution was sufficient to resolve some of the deuterium-deuterium dipolar interaction between pairs of methylene deuterons, and in 40·7 and 60·7 also between the methyl deuterons. A further improvement in the resolution was achieved by using a double quantum spectroscopic technique recently developed in this laboratory.⁴³⁻⁴⁵ With this method "long range" dipolar interaction of the type α - γ could be resolved. The dipolar structure of the spectrum in both the single and double quantum regimes is described in Section IV. Finally in Sections V and VI we describe the temperature dependence due to the alkoxy chain deuterons for all compounds over the whole liquid crystalline region. It is shown that both the quadrupolar and dipolar interaction constants decrease along the chain towards its end in a typical stepwise fashion. These results are interpreted in terms of conformation equilibria of the chain structure. It is shown that they are consistent with a dynamic model in which kink deformations are the major structural defects of the chain, with a probability distribution which increases monotonically towards its methyl end. These deformations are rapidly equilibrated by zipping up and down the alkoxy chain. The characteristic stepwise decrease in the splitting constants along the chain results from a combined effect of the above dynamic model and an assumed rod-like structure for the liquid crystal molecules, in which the chain axis is tilted with respect to the long molecular axis. Using this model we estimate quantitatively the kink probability distribution in the various chain segments.

II. EXPERIMENTAL

A. Materials

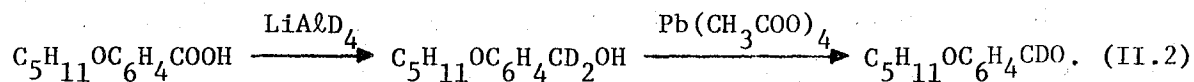
All compounds studied were of type no.7 with $n = 4, 5, 6,$ and 7 . The compounds were synthesized by mixing equimolar amounts of p-n-heptylaniline (commercial grade) with various isotopically labeled species of p-n-alkoxybenzaldehyde in absolute ethanol, refluxing for four hours, and purifying by repeated crystallization from 95% ethanol.

The (isotopically labeled) p-n-alkoxybenzaldehydes were synthesized from p-hydroxybenzaldehyde and the corresponding 1-bromoalkanes according to⁴⁶

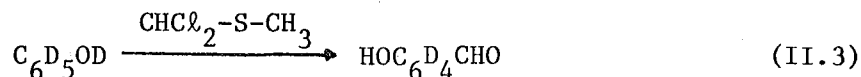


For the no.7 compounds, perdeuterated in the alkoxy chain, commercial (Merck, Sharp & Dohm) perdeuterated 1-bromoalkanes, $\text{C}_n\text{D}_{2n+1}\text{Br}$, were used.

Several no.7 compounds deuterated specifically in either the benzylidene group or the alkoxy chain were prepared from the corresponding deuterated alkoxybenzaldehyde: The methine deuterated compound was prepared by reducing p-n-pentyloxybenzoic acid (Eastman) with LiAlD_4 to the corresponding alcohol-d₂ followed by oxidation to the aldehyde-d₁ with lead tetraacetate,⁴⁷

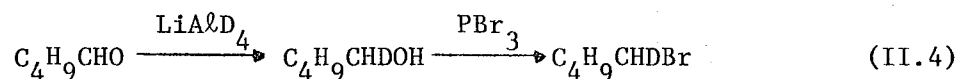


Phenyl-d₄-pentyloxybenzaldehyde was prepared from perdeuterated phenol (Stohler Isotopes) by converting it to p-hydroxybenzaldehyde with dichloromethylene sulphide⁴⁸

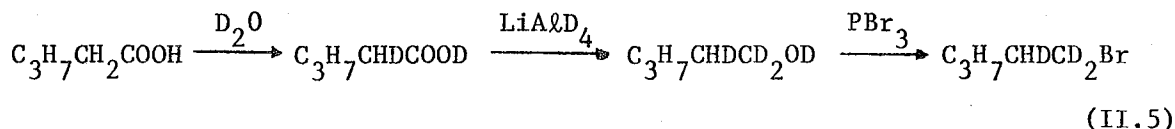


and proceeding according to (II.1).

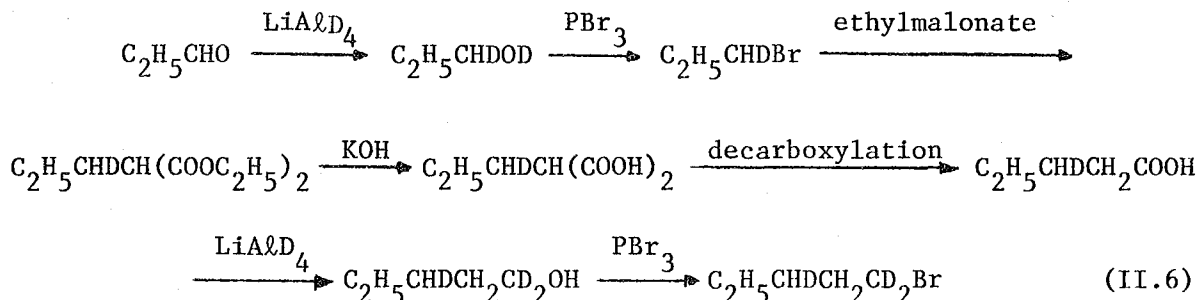
The 50.7 compounds specifically deuterated in the pentyloxy chain were synthesized from the corresponding deuterated 1-bromopentane: α -d₁-1-bromopentane was prepared by reducing valeraldehyde with LiAlD₄⁴⁹ followed by bromination with PBr₃⁵⁰



$\alpha_2\beta$ -deuterated 1-bromopentane was prepared by exchanging the α protons of pentanoic acid with D₂O⁵¹ to the desired amount (\sim 15% in the compound used), followed by reduction with LiAlD₄ and bromination:



$\alpha_2\gamma_1$ -d₃-1-bromopentane was synthesized from propionaldehyde by the following sequence, where the chain elongation step was according to reference 52;



All major intermediates and final products were analyzed massspectrometrically and gave the expected isotopic constitution.

The high resolution deuterium NMR spectra of the four no.7 perdeuterated in the alkoxy chains, in the isotropic phase, are shown in Figure 1. In all spectra the relatively weak and broad signal, at the low field end, corresponds to the α deuterons, and the intense sharp peak near the high field end corresponds to the methyl deuterons. The other methylene groups are resolved in the 40.7 spectrum and partly in the 50.7 spectrum, but not in 60.7 and 70.7. In the latter case the resolution is hampered by the large number of methylene groups and also by the higher viscosity of this compound.

B. NMR Measurements

The liquid crystalline samples (~ 0.8 gr) were placed in 7 mm o.d., 6 mm i.d. and 20 mm long pyrex tubes. The liquid crystal was degassed by repeated freeze-thaw and sealed off under vacuum.

The NMR spectrometer used to record the spectra⁵³ consisted of a Bruker 43 Kgauss superconducting magnet, corresponding to 28 MHz for ^2D and 180 MHz for ^1H . The (single quantum) deuterium spectra were obtained by Fourier transformation of the FID signal following a 90° pulse, under condition of proton decoupling. Typical H_1 for the deuterium pulses were about 80 gauss ($\tau_{90} \sim 5 \mu\text{s}$) and the proton decoupling field H_2 was set at about 8 gauss. Usually 30 to 100 FID signals were accumulated to improve the signal to noise with interval between pulses of about 3 sec. The number of frequency points per spectrum was 1024.

The double quantum (D.Q.) spectra were obtained by a two dimensional Fourier transform technique, according to method C described in Figures 20 and 23 of reference 44. The experiment consisted of two pulses: a

weak preparation pulse of 90° in the D.Q. regime, adjusted to a particular quadrupole doublet, followed, after a time τ , by a single quantum (S.Q.) detection pulse of 90° . The D.Q. spectrum is obtained by first Fourier transforming the FID signal following the S.Q. 90° pulse, and then the integrated intensity of one quadrupole component of the desired signal is Fourier transformed with respect to τ . As for the S.Q. case all D.Q. spectra were recorded in the presence of proton decoupling and usually 30 to 100 signals were accumulated to improve the signal to noise ratio.

The sample temperature was regulated by a stream of heated nitrogen, using a copper constantan thermocouple to monitor and regulate the temperature. The temperature stability was better than $\pm 0.1^\circ\text{C}$ during measurements and its accuracy is estimated at $\pm 1^\circ\text{C}$.

All spectra were recorded by first heating the sample to the nematic phase, letting it equilibrate for several hours and then cooling it, in small steps, through the various mesophases. In all measurements the sample orientation relative to the external field was kept unchanged, i.e., with the director parallel to the external magnetic field.

III. DEUTERIUM NMR IN THE MESOMORPHIC PHASES AND PEAK ASSIGNMENT

An exact interpretation of the NMR spectrum of spin $I = 1$ nuclei in liquid crystals is quite complicated and requires excessive experimental data and computations. We shall therefore adopt certain approximations which will significantly simplify the interpretation of the results. These approximations which are often employed for deuterium NMR in liquid crystals are¹²: (i) the deuterium quadrupole tensor is assumed to be axially symmetric with the unique axis parallel to the C-D bond direction, (ii) the various mesophases can be considered (at least locally) uniaxial, and each conformation of the liquid crystal molecules can be approximated to a rigid cylindrical rod whose symmetry axis is parallel to the "molecular long axis". Under these conditions only a single orientational order parameter, S , is needed to describe the molecular ordering, and the spin Hamiltonian of the deuterium becomes

$$\mathcal{H} = -\nu_0 \sum_i I_z^i + \sum_i \nu_q^i (I_z^i)^2 + \sum_{i < j} D^{ij} \left[I_z^i I_z^j - \frac{1}{4}(I_+^i I_-^j + I_-^i I_+^j) \right] \quad (\text{III.1})$$

where

$$\nu_0 = \gamma_D H_0 / 2\pi \quad (\text{III.2})$$

$$\nu_q^i = q \cdot S \cdot Y(\theta_q^i) = \frac{3}{4} \frac{e^2 q Q}{h} \cdot S \cdot Y(\theta_q^i) \quad (\text{III.3})$$

$$D^{ij} = d^{ij} \cdot S \cdot Y(\theta_d^{ij}) = -\frac{\gamma_D^2 h}{2\pi^2 (r^{ij})^3} \cdot S \cdot Y(\theta_d^{ij}) \quad (\text{III.4})$$

$$Y(\theta) = Y_0^2(\cos\theta) = \frac{1}{2} (3 \cos^2 \theta - 1) \quad (\text{III.5})$$

In these equations θ_q^i and θ_d^{ij} are respectively the angle between the C-D bond of the i^{th} deuterium and the angle between the radius vector r^{ij} connecting nuclei i and j , and the "molecular long axis" which we designate by L . The three terms in Eq. (III.1) are respectively the Zeeman energy, quadrupole interaction and deuterium-deuterium dipolar interaction. We have neglected the chemical shift and the indirect spin-spin coupling interactions since for deuterium they are too small to affect the spectrum in liquid crystals. Also since the spectra are recorded under condition of proton spin decoupling, no term due to deuterium-proton dipolar interaction is included.

Deuterium quadrupole interaction constants, q , in C-D bonds usually range³⁶ between 150 and 200 KHz. For deuterons bonded to unsaturated carbons this interaction averages around 185 KHz, while for aliphatic deuterons the average is around 168 KHz. We shall use these figures in our calculations below. Deuterium-deuterium dipolar couplings, d^{ij} , are much smaller than the quadrupolar interaction. For example, for two deuterons 2 \AA apart a value of $d^{ij} = -0.7 \text{ KHz}$ is calculated. Since the deuterium NMR linewidth in liquid crystals is usually several hundred hertz wide, dipolar splittings are often not resolved. Thus the DMR spectrum of a deuterated liquid crystal consists essentially of a doublet for each type of deuterium of magnitude

$$\Delta^i = 2 \nu_q^i = \frac{3}{2} \frac{e^2 q Q}{h} S \cdot Y(\theta_q^i) \quad , \quad (\text{III.6})$$

and depending on the circumstances, possibly also fine structure due to dipolar couplings between neighboring deuterons. The detailed dipolar

structure depends on the relative values of D and ν_q .

In Figure 2 are shown typical examples of the deuterium NMR spectra of the four no-m compounds studied. The compounds used to record these spectra were perdeuterated in their alkoxy chains, and as expected, the spectra usually consist of n distinguishable quadrupolar doublets. On the scale of this figure some components are not resolved, but on a wider scale they can often be separated. Many of the quadrupole components exhibit fine structure which we attribute to deuteron-deuteron dipolar interaction within the methylene or methyl groups. We discuss this structure in more detail in Section IV below. In all cases the CD_3 signal can be identified from its relative intensity ($3/2$ compared to the other signals), and sometimes by its dipolar structure. This signal is always found to be the innermost doublet. The other signals correspond to the CD_2 deuterons, but no a priori assignment to particular methylene-segments in the alkoxy chain is possible from these spectra alone.

An unambiguous assignment for the methylene signals was established for 50.7, by using a number of specifically deuterated species of this compound. The DMR of these species are shown in Figure 3. The upper trace in this figure corresponds to a compound in which 15% of the β protons were randomly exchanged with deuterons while the α methylene was completely deuterated. This preparation therefore contains $\sim 72\%$ $\alpha_2-d_2-50.7$, $\sim 25\%$ $\alpha_2\beta_1-d_3-50.7$ and less than 3% $\alpha_2\beta_2-d_4-50.7$. Thus the position of the α -deuterons (center of gravity of the three intense high field dipolar components) and the β -deuterons (low field weak peak) are established. The second trace corresponds to the $\alpha_2\gamma_1-d_3-50.7$, thus allowing the identification of the peak due to γ -deuterons and by comparison with the third trace of

the perdeuterated chain (which also contains some methine- d_1 -50.7) the position of the δ methylene (and methine) is established.

Thus the assignment of the alkoxy methylene signals of 50.7 shows that the quadrupole splitting decreases along the chain from the benzylidene ring towards the end methyl group. This behavior was indeed assumed previously to obtain for aliphatic chain deuterons in other thermotropic liquid crystals,¹⁷ and we shall assume that the same trend of quadrupolar splitting occurs also in the other no.7 compounds studied.

We have also studied the deuterium resonance of the benzylidene ring in the isotopic species pentyloxy(phenyl- d_4 -benzylidene)-heptylaniline. A typical spectrum is shown in the bottom trace of Figure 3. There are two quadrupole doublets corresponding to ortho and meta deuterons (with respect to the alkoxy chain), each splits into three by the direct dipolar interaction between them. We discuss the dipolar structure of this spectrum in the next sections below. On the basis of this spectrum alone it is not possible to assign the deuteron signals to particular ring positions. But by analogy with the works of Diehl and Tracey¹³ and Dong et al.,¹⁹ on PAA and MBBA, we associate the inner quadrupole component with the deuterons ortho to the alkoxy group and the outer component with the meta-deuterons. This assignment is also supported by the fact that proton decoupling had a larger narrowing effect on the inner component ascribed to the ortho-deuterons which are expected to be more strongly coupled by dipolar interaction to the chain protons.

IV. DIPOLAR STRUCTURE IN THE SINGLE AND DOUBLE QUANTUM SPECTRA

As indicated above many of the quadrupole components exhibit fine structure due to deuteron-deuteron dipolar interaction. In the (single quantum) spectra of Figures 2 and 3 three types of dipolar interactions are observed: (i) between methylene deuterons (type A_2), (ii) between the inequivalent aromatic deuterons (type AB) and (iii) between the three equivalent deuterons in the methyl group (type A_3). Dipolar interactions between different methylene groups are too small to resolve in the normal, single quantum, spectrum. The resolution could however be improved by employing the method of double quantum spectroscopy which allowed determination of dipolar splitting between different methylene groups. In this section we first discuss the dipolar structure in the normal (S.Q.) spectra, and then present some results obtained by D.Q. spectroscopy.

A. Normal (S.Q.) spectra

The best resolved spectra of type A_2 were obtained in $\alpha_2\text{-d}_2\text{-50.7}$ (mixed with some $\alpha_2\beta_1\text{-d}_3\text{-50.7}$). An expanded spectrum of the high field component of this species is shown in Figure 4a. The theory of the A_2 case with $I = 1$ predicts¹² that, for $D \ll \nu_Q$, each of the quadrupole components splits into three lines with relative intensities 2, 3, and 1. The corresponding frequencies are respectively $\frac{3}{2} D$, $-\frac{1}{2} D$, and $-\frac{3}{2} D$ relative to the $-\nu_Q$ component, and $-\frac{3}{2} D$, $\frac{1}{2} D$ and $\frac{3}{2} D$ relative to the $+\nu_Q$ component. The α -deuterons spectrum in Figure 4a is consistent with this structure only if D and ν_Q are assumed to have opposite signs. Thus interpretation of the methylene spectra yield both the magnitude of D

and its relative sign with respect to the quadrupolar interaction.

In Figures 4b and 4c are shown spectra of the α -deuterons region for other 50.7 species recorded on the same scale and at nearly the same temperature as the spectrum in trace a of that figure. These spectra correspond to the species $\alpha_2\gamma_1-d_3$ and perdeuterated alkoxy chain respectively. There is a clear increase in linewidth on going from spectrum a to b to c. Since all spectra were recorded under similar conditions, in particular proton decoupling, the excess width in the spectra of $\alpha_2\gamma_1-d_3$ and perdeuterated 50.7 must be attributed to the unresolved dipolar interaction between deuterons on different carbon atoms. We shall return to this point in the second part of this section.

From the isotropic spectra in Figure 1 we estimate a contribution to the (full) linewidth (at half maximum intensity) from field inhomogeneity of at most 10 or 20 Hz while the linewidths in the spectrum of trace a, which is essentially due to $\alpha_2-d_2-50.7$, is about 150 Hz. This is about the same linewidth obtained for the deuterium signal in methine- $d_1-50.7$ (see Figure 4d) where no dipolar interactions are present at all. We ascribe this residual width to imperfect alignment of the director in the sample resulting in small distribution of the quadrupole splitting. Using the approach of reference 3 a distribution of $\pm 2^\circ$ in the director's alignment can be estimated from the observed linewidth of traces 4a and 4d.

The structure of the benzyldene ring deuterium resonance is shown on an expanded scale in trace e of Figure 4. This spectrum can be quantitatively interpreted in terms of an AB spin $I = 1$ system, where the splitting comes from dipolar interaction between the deuterons

ortho and meta to the alkoxy chains. The interaction between deuterons on opposite sides of the benzene ring is apparently too small to affect the spectrum. The general theory for the AB case is given in Appendix A where it is shown that when $|D| \ll |v_Q^A + v_Q^B|$, $|D| \lesssim |v_Q^A - v_Q^B|$ ($D = D^{AB}$), and assuming v_Q^A and v_Q^B to have the same sign, each quadrupole component splits into three lines of unequal intensities; $1, (\sin\alpha + \cos\alpha)^2$ and $(\sin\alpha - \cos\alpha)^2$ at frequencies $-D-\epsilon$, $-\epsilon$ and $D-\epsilon$ relative to v_Q^A , and $1, (\sin\alpha - \cos\alpha)^2$ and $(\sin\alpha + \cos\alpha)^2$ at frequencies $-D+\epsilon$, ϵ and $D+\epsilon$ relative to v_Q^B , where $\epsilon = (\frac{1}{2} D)^2 / (v_Q^B - v_Q^A)$ and $\tan 2\alpha = 4\epsilon/D$. The stick diagram in trace 4d gives the transition frequencies and intensities as calculated from the above expression, and taking the same signs for D and the v_Q 's.

As may be seen in Figure 2, there is also some fine structure in the methyl resonances of 40.7 and 60.7. This is more clearly shown in Figure 4f where the methyl resonance of 40.7, perdeuterated in the alkoxy chain, is reproduced on a much larger scale. This structure results from the dipolar interaction between the three equivalent deuterons of the methyl group. The relevant theory is given in Appendix A. It shows that each quadrupole component should split into seven lines, as shown by the stick diagram accompanying the spectrum in Figure 4f. The resolution in this case is not sufficient to bring out all the transitions, however the overall lineshape can readily be reproduced, using line simulation programs, by introducing appropriate linewidths.

In practice in most cases where perdeuterated chains were used, the dipolar structure was only partially resolved due to the excess linewidth, which ranged between 200 and 600 Hz (depending on the phase

and temperature). To obtain the dipolar interaction the experimental results were best fitted to simulated spectra with varying D and linewidth.

B. Double quantum spectra

In a few cases we were able to improve the resolution of the spectrum, and thus obtain long range deuterium-deuterium dipolar interaction, by using a double quantum spectroscopic method, recently developed in this laboratory by Pines and co-workers.⁴³⁻⁴⁵ We refer to the original literature for the details of the method. Basically, by using a judiciously chosen pulse sequence it is possible to obtain (by a two dimensional Fourier transformation) a spectrum corresponding purely to $\Delta m^i = 2$ transitions for the group of equivalent nuclei i . We refer to this spectrum as the double quantum spectrum. To first order in ν_Q/ν_0 the D.Q. spectrum is independent of ν_Q , although the dipolar interaction (and the chemical shift) still affect its structure. Since, as described in Section III, the distribution in the quadrupolar splitting is the dominant contribution to the linewidth of the S.Q. spectrum we hoped to increase the resolution by recording D.Q. spectra of some specifically deuterated species. In practice we succeeded in two cases.

The first case is the α -resonance of α_2 -d₂-50.7 (the same compound used to record the upper trace in Figure 3 and trace a in Figure 4). The D.Q. spectrum of this signal consisting of a 1:1:1 triplet of equal spacing is shown on the right-hand side of the upper traces in Figure 5. From the energy level diagram of two equivalent nuclei of spin $I = 1$ ¹² one readily finds that there should be three $\Delta m^i = 2$ transitions of

equal intensities, at 0 and $\pm 2D$ relative to the central D.Q. frequency (see Appendix B). Comparison of the S.Q. and D.Q. spectra in the upper traces of Figure 5, which correspond to the same compound and were recorded under the same experimental conditions, shows complete agreement for the value of D in both spectra. Moreover, the linewidth in the D.Q. spectrum is indeed smaller than in the S.Q. spectrum, but it is still larger than that expected from the field inhomogeneity. (The contribution of field inhomogeneity to the linewidth of the D.Q. spectrum is twice that in S.Q. spectroscopy, i.e., in our case we expect a linewidth of at most 40 Hz compared to ~ 100 Hz obtained experimentally.) We also do not understand the linewidth variation in the D.Q. spectrum of Figure 5a.

The second case is the γ resonance of $\alpha_2\gamma_1\text{-d}_3\text{-50}\cdot 7$ (second trace in Figure 3). The S.Q. and D.Q. spectra of this signal for two different temperatures are shown on an expanded scale in the middle and lower traces of Figure 5. Although no structure is observed in the S.Q. spectra a clear splitting into a 1:2:3:2:1 quintuplet is seen in the corresponding D.Q. spectra. The deuterons of the $\alpha_2\gamma_1\text{-d}_3$ isotopic species form a AA'B system which is solved (for the limit $D^{ij} \ll v_q^i, v_q^j$) in the third part of Appendix A, and for the D.Q. spectrum in the second part of Appendix B. The calculated spectra depend on the relative magnitude of the D^{ij} 's; $D^{AA'} = D^{\alpha\alpha}$, $D^{AB} = D^{\alpha_1\gamma}$ and $D^{A'B} = D^{\alpha_2\gamma}$. When $RD = D^{\alpha_1\gamma} - D^{\alpha_2\gamma} \ll D^{\alpha\alpha}$, the expected D.Q. spectrum (Table XII) reduces to a 1:2:3:2:1 quintuplet with spacing $SD = D^{\alpha_1\gamma} + D^{\alpha_2\gamma}$. This is the type of D.Q. spectrum indeed observed for the γ -deuterons in $\alpha_2\gamma_1\text{-d}_3\text{-50}\cdot 7$.

Thus only the sum SD can be determined experimentally. The stick diagrams for the γ resonances in Figure 5 (for both the S.Q. and D.Q. spectra) were calculated using the following parameters $SD/D^{\alpha\alpha} = 0.62$, and $RD/D^{\alpha\alpha} = 0.15$. These parameters were obtained from the analysis of the quadrupolar splittings as described below.

Attempts to obtain resolved D.Q. spectra of the methyl or methylene signals in no.7 compounds with perdeuterated alkoxy chains failed. We believe that this is due to the large number of interactions between neighboring methylene groups resulting in a too large number of transitions to be resolved even in the D.Q. spectrum (at least at its present degree of development). We were also unable to obtain resolved D.Q. spectra for the β signal in $\alpha_2\beta_1\text{-d}_3\text{-50.7}$, apparently because of interference with the strong signal from the α -deuterons of $\alpha_2\text{-d}_2\text{-50.7}$ during the D.Q. free induction decay.

V. QUADRUPOLAR SPLITTING AND MOLECULAR ORDERING

Except for some isotopic species of 50•7 discussed above, the no•m compounds studied in the present work were all perdeuterated in their alkoxy chains. Typical spectra of all the compounds studied, for each of their various mesophases, are shown in Figures 6-9. The (full) quadrupolar splitting ($\Delta = 2\nu_Q$) and dipolar interaction between the methylene deuterons, D (calculated from considerably more expanded spectra than those shown in Figures 6-9) are plotted in Figures 10-13 as function of temperature, over the whole liquid crystalline region of the various compounds. As indicated in Section IV the analysis also gives the sign of D/ν_Q ; this is always negative for the CD_2 and CD_3 groups and positive for the benzylidene deuterons.

The main features of these results are similar to those found previously in other thermotropic liquid crystals.^{12,17} There is a relatively strong temperature dependence of ν_Q in the nematic and smectic A phases, while in the smectic B phases the splitting is quite independent of temperature. First order phase transitions are usually accompanied with discontinuities in the ν_Q and D plots, although in some cases these are too small to notice on the scale of the figures. In addition there are some typical features characteristic of the chain nuclei:

(i) The methylene splittings exhibit a gradual decrease of Δ along the chain with pairwise clustering such that

$$\Delta^2 \gtrsim \Delta^3 \gg \Delta^4 \gtrsim \Delta^5 \gg \Delta^6, \text{ etc.}, \quad (\text{V.1(a)})$$

where the superscript indicates the numbering of the atom in the chain (including oxygen) from the benzylidene end. (ii) The end methyl splitting is smaller than all methylene Δ^i 's in the same compound, but varies in an alternating way from one compound to another; it is relatively large for odd membered chains (40·7 and 60·7) and very small for even membered chains (50·7 and 70·7). In the latter case it sometimes exhibits anomalous temperature dependence, i.e., the splitting increases with increasing temperature. (iii) The dipolar interaction between the methylene deuterons exhibit similar pairwise clustering as do the Δ^i 's, i.e.,

$$D^{\alpha\alpha} \sim D^{\beta\beta} \gg D^{\gamma\gamma} \sim D^{\delta\delta} \gg D^{\epsilon\epsilon}, \text{ etc.} \quad (\text{V.1(b)})$$

and they are roughly proportional to the latters with negative D^{ii}/Δ^i . The overall measureable range of the D's is however quite limited. For the methyl group the ratio D/Δ (in 40·7 and 60·7, where D could be measured) is essentially constant for all phases at about -6×10^{-3} (see Table II).

The pairwise clustering of the methylene splitting and the alternating values of the Δ^{CD_3} were observed previously in other thermotropic and lyotropic liquid crystals¹⁴⁻¹⁷ and have been referred to as "even-odd" effects. In the next section we propose a model to explain these effects and use the results to derive information about chain conformation. Here we concentrate on the benzylidene deuteron data of 50·7, and analyze the results in terms of the structure and the ordering of the aromatic part of the molecule.

Assuming a rigid, and for simplicity, also a coplanar structure for the benzylidene aniline moiety, we may associate it with a "long axis", L, as indicated in the molecular diagram in Section I. Because of the fast rotation of the benzene rings about their para axis the two ortho and two meta deuterons in each ring are magnetically equivalent, but at least for the benzylidene deuterons their quadrupole splittings differ somewhat as a result of a slight distortion of the CCD angle from 120°. ^{12,19} An estimate for the angle α , between L and the phenyl para axis, and for the molecular order parameter S, can be obtained from the benzylidene ring and methine spectra using Eqs. (III.3)-(III.6) in two independent ways: (i) From the methine, Δ^{CD} , and aromatic, Δ^{ar} , quadrupolar splittings, using the relation ¹²

$$\frac{\Delta^{CD}}{\Delta^{ar}} = \frac{Y(60+\alpha)}{\frac{1}{2}[Y(60+\alpha) + Y(60-\alpha)]} \quad (V.2)$$

and (ii) from the ratio of the dipolar interaction between the ortho and meta ring nuclei, D, and their quadrupolar splitting:

$$\frac{D}{\Delta^{ar}} = \frac{d \cdot Y(\alpha)}{q \cdot \frac{1}{2} [Y(60+\alpha) + Y(60-\alpha)]} \quad (V.3)$$

For the actual calculations we used for Δ^{ar} the larger of the two benzylidene splitting since it is believed to result from deuterium meta to the alkoxy chain which are less distorted from hexagonal symmetry. ¹³ Taking the distance between the ortho and meta deuterons as 2.48 Å, $q = 185 \text{ KHz}$

(for the aromatic and methine deuterons) and the experimental results of Figure 11, Eqs. (V.2) and (V.3) give the results for α plotted in the upper part of Figure 14. Once α is known, S can be calculated from either the quadrupole or the dipolar interactions of the ring deuterons. The results calculated from the two sets of data are plotted in the lower part of Figure 14. As may be seen in this figure the values derived for α by the two methods are quite similar and constant, ranging between 9 and 12°. The average value of 10° for α is close to results obtained in other systems.^{11,12}

The agreement between the two sets of data for the order parameter S is less satisfactory. This is probably due to the simplified assumption made about the molecular structure and symmetry. The general behavior of the curves, is however quite similar and is clearly related to the molecular ordering in the various phases. The strong temperature dependence in the nematic range is typical to this phase. The results show however that the ordering parameter is also quite temperature dependent in smectic A and C, while in the smectic B phases it is constant and close to its maximum possible value of unity. This reflects the fact that in these phases the distribution of the long axis of the molecules deviate very little from the director. Since the deuterium, NMR lines remain relatively sharp over the whole mesomorphic range, it follows that the reorientational rate about the molecular axis and the translational diffusion remain fast in all phases (on the NMR time scale).

VI. THE ALKOXY CHAIN

The main part of this work is concerned with the deuterium splittings in the alkoxy chains. We discuss this problem in the present section which is divided into three. First, we describe a model that explains the characteristic splitting pattern of the methylene deuterons. Next, we discuss the methyl splitting whose behavior is somewhat different from that of the methylene, and finally we use the model with the experimental results in order to obtain quantitative information on the alkoxy chain conformational equilibria.

A. The Methylene Groups

If the alkoxy chains had a rigid all-trans configuration as shown on the left-hand diagram of Figure 15, then we would expect for all methylene deuterons identical Δ^i 's and CD_2 -dipolar interactions. In fact as indicated above for all compounds and in all phases there is a gradual decrease in both the quadrupolar and dipolar splitting with characteristic pair clustering as shown in Eqs. (V.1). Typical plots of the methylene Δ^i 's for the various phases of the compounds studied as function of the position along the chain are shown (full points) in Figures 16 and 17. The decrease of Δ along the chain is usually attributed to fast reorientational isomerism. As we show below the characteristic stepwise decrease of the Δ^i 's along the chains allows us to be more specific about this isomerization equilibria. It is shown that this effect is a consequence of a number of factors; (i) The dominant structural defect in the all trans chain is the formation

of "kinks", (ii) the chain axis is inclined to the molecular long axis, and (iii) the probability for structural defects increases monotonically along the chain towards the end methyl group.

Clearly the most stable chain conformation is the all-trans state, for which the internal energy of the chain is minimum and in which the molecules fit best into the ordered structure of the liquid crystalline phases. The most abundant structural defect is expected to be the so-called "kink" (and to a less extent "jog") defined by the sequence $tt\dots tg^{\pm}tg^{\mp}tt\dots$ (and $tt\dots tg^{\pm}ttg^{\mp}tt\dots$) where t refers to a trans segment and g^{\pm} to a \pm gauche segment.^{25,26,54,55} This assumption is based on the fact that kinks perturb least the parallel arrangement of the molecules in the mesophases. In the center and right diagrams of Figure 15 are shown alkoxy chains with a single kink. We distinguish between "even kinks" in which the first gauche atom in the kink (counted from the benzylidene end) is an even numbered atom, and "odd kinks" in which the first gauche atom is an odd numbered carbon. It may be seen in these two diagrams that two out of the four C-D bonds of the kink (the first gauche and next trans carbons) change their orientation relative to the molecular axis, L , compared to the C-D orientation in the all-trans segments. Moreover the new orientations of the C-D bonds in the even kinks are different from those in odd kinks. This is depicted in more detail in Figure 18 which shows a bond diagram of an even carbon atom in the trans chain. Bonds (1) and (2) represent C-C bonds in the figure's plane while bonds (3) and (4) represent C-D bonds in and out of the plane. Referring again to Figure 15

we note that in an even kink at atom i , one C-D bond on each of carbons i and $i + 1$ transforms from type (3) (or 4) into type (1) bond, while for an odd kink at atom i , a C-D bond on each of carbons i and $i + 1$ will transform into a bond of type (2). Since bonds (1) and (2) make in general different angles with L , even and odd kinks will have different effects on the deuterium quadrupolar (and dipolar) splitting. To put these arguments on a quantitative basis we need the angles between L and the various bond types. We assume that in all conformations

$$\angle \text{CCC} = \angle \text{DCD} = \tau = 109.47^\circ$$

where τ is the tetrahedral angle. The angle α' between L and bond (1) then is:

$$\alpha' = \alpha + (\angle \text{COC} - \angle \text{CCC})$$

where $\angle \text{COC}$ is the angle between the two O-C bonds at the alkoxy oxygen. In a number of aromatic alkoxy compounds this angle was determined by x-ray crystallography, and was found to range between 115° and 125° , depending on the compound.⁵⁶ Thus α' should lie in the range 15° to 25° . The angle of the other bonds with L depend on α' as shown in Figure 18.

If, we consider only the kink-distortions and assume that they equilibrate rapidly on the NMR time scale with the all-trans conformations,⁵⁴ then the quadrupolar splitting of the deuterons bonded to an even carbon is

$$\Delta^i = 2q \cdot S \cdot \left[\left(1 - \frac{1}{2} P^i - \frac{1}{2} P^{i-1} \right) Y(\theta_q^3) + \frac{1}{2} P^i Y(\theta_q^1) + \frac{1}{2} P^{i-1} Y(\theta_q^2) \right]$$

(VI.1)

and for deuterons bonded to odd atoms

$$\Delta^i = 2q \cdot S \cdot \left[\left(1 - \frac{1}{2} P^i - \frac{1}{2} P^{i-1} \right) Y(\theta_q^3) + \frac{1}{2} P^i Y(\theta_q^2) + \frac{1}{2} P^{i-1} Y(\theta_q^1) \right] \quad (\text{VI.2})$$

where θ_q^k is the angle that the bond type k makes with L , and P^i is the probability of a kink, both of type g^+tg^- and g^-tg^+ , at atom i . The factor $\frac{1}{2}$ results from the fact that the orientation of only one of the two methylene deuterons is influenced by kink formation, but both deuterons are affected by the same amount since the probability of a left kink, g^+tg^- , is the same as for a right kink, g^-tg^+ . It should be noted that in Eq. (VI.1) and (VI.2) it is assumed that the magnitude of the order parameter S , and the orientation of L in the molecule (i.e., relative to the aromatic core) are the same for the all-trans and the kinked conformation.

Similar equations can also be written for the dipolar interaction between deuterons in the chain. The equations for the dipolar interaction between the equivalent methylene nuclei bonded to even atoms are:

$$D^{ii} = d^{CD_2} \cdot S \cdot \left[(1 - P^i - P^{i-1}) Y(\theta_d^{34}) + P^i Y(\theta_d^{14}) + P^{i-1} Y(\theta_d^{24}) \right] \quad (\text{VI.3})$$

and for odd atoms:

$$D^{ii} = d^{CD_2} \cdot S \cdot \left[(1 - P^i - P^{i-1}) Y(\theta_d^{34}) + P^i Y(\theta_d^{24}) + P^{i-1} Y(\theta_d^{14}) \right] \quad (\text{VI.4})$$

where $\theta_d^{k\ell}$ is the angle between L and the radius vector $r^{k\ell}$ connecting two methylene deuterons in bonds of type k and ℓ respectively. In applying Eqs. (VI.1)-(VI.4) we shall assume that the oxygen ether group remains coplanar with the benzylidene ring in all conformations, i.e., we take $P^1 = 0$. Equations (VI.1) and (VI.3) for the deuterons on the α -carbon then simplify respectively to:

$$\Delta^2 = 2q \cdot S \cdot \left[\left(1 - \frac{1}{2} P^2\right) Y(\theta_q^3) + \frac{1}{2} P^2 Y(\theta_q^1) \right] \quad (\text{VI.1a})$$

and

$$D^{22} = d^{CD_2} \cdot S \cdot \left[(1-P^2) Y(\theta_d^{34}) + P^2 Y(\theta_d^{14}) \right] \quad (\text{VI.3a})$$

In Table III are summarized the expressions for θ_q^k and $\theta_d^{k\ell}$ in terms of the angles α' and τ . Some numerical values of θ and $Y(\theta)$ for a number of α' values are also given.

It is clear that when the chain axis is parallel to L, i.e., $\alpha' = \frac{1}{2}(\pi - \tau) = 35.26^\circ$ the effect of even and odd kinks would be the same, since in this case bonds (1) and (2) become equivalent and the coefficients in the above equations of P^i and P^{i-1} become identical. Also if the kink probabilities were constant along the chain all methylene deuterons (except for the first) would have the same Δ (and D) values (as can readily be asserted by setting $P^i = P^{i-1}$ in the above equations). The general pattern of the results for Δ^i clearly indicates that this is not the case and that rather P^i increases along the chain.

To demonstrate the effect of varying P^i on Δ we show in Figure 19, calculated quadrupole splittings of methylene deuterons for 5, 6, 7

and 8 membered alkoxy chains, using Eqs. (VI.1) and (VI.2). For the calculations we used several α' values between 10° and 25° , and assumed a linear increase in P^i with i according to

$$P^i = 0.05 + 0.06(i - 2) \quad (i \geq 2) \quad (\text{VI.5})$$

We arbitrarily choose S such that $\Delta^2 = 1.0$. The results clearly bear out the main feature of the methylene splitting, i.e., the stepwise decrease in Δ along the chains (cf. open circles and broken lines in Figures 16 and 17).

Of course one could easily simulate this pattern of Δ , without resorting to geometrical consideration, by assuming an "even-odd" effect for the kink probabilities, i.e., assume that P^i for an even atom is larger than for the next (odd) atom. However, there seems to be no reason, structural or otherwise, why this should be so. Also introduction of other structural defects into the calculations, such as a "bent" (single gauche) or a "jog" affects the results of many more deuterons in the chain than does a single kink and causes a smearing out of the characteristic steps of Figure 19. For these reasons we believe that the splitting pattern of the methylene deuterons must result from the three factors considered, i.e., (i) formation of kink defects along an aliphatic chain whose (ii) axis is inclined to the molecular axis, L , and (iii) with probability that increases monotonically along the chain.

Before attempting to use this picture to calculate the P^i 's from the actual results we discuss briefly the splitting pattern of the end methyl groups.

B. The Methyl Groups

The fast rotation of the methyl groups about their C_3 axes results in partial averaging of their quadrupolar and dipolar interactions.¹⁰ The principal direction of the average tensors are parallel to C_3 , and assuming a tetrahedral structure, the interaction constants become respectively

$$\nu_q^{CD_3} = \frac{3}{4} \frac{e^2 q Q}{h} \cdot S \cdot Y(\tau) \cdot \overline{Y(\theta_q^{CD_3})} = -\frac{1}{3} q \cdot S \cdot \overline{Y(\theta_q^{CD_3})} \quad (VI.6)$$

and

$$\Delta_D^{CD_3} = -\frac{\gamma_D^2 h}{2\pi r^3} S \cdot Y\left(\frac{\pi}{2}\right) \cdot \overline{Y(\theta_q^{CD_3})} = -\frac{1}{2} d^{CD_3} \overline{S \cdot Y(\theta_q^{CD_3})} \quad (VI.7)$$

where $\theta_q^{CD_3}$ is the angle between the C_3 axis and L, and the bar indicates averaging over all orientations of the C_3 axis. Thus the ratio between the quadrupole splitting and dipolar interaction constants for the methyl group should be a constant independent of the molecular conformation,

$$\frac{\Delta_D^{CD_3}}{d^{CD_3}} = \frac{4}{3} \frac{q}{d^{CD_3}} = -169 \quad (VI.8)$$

where we used 1.786 Å for the interdeuteron distance and 168 kHz for the quadrupole interaction constant of the C-D bond. In Table II are given experimental results for this ratio, for those compounds and phases where the methyl dipolar interaction was resolved. As may be seen the results are in complete agreement with the prediction of Eq. (VI.8).

The alternating splitting of the CD_3 deuterons along the homologous series follows from the alternating orientation of the C_3 axis relative to L. If we consider the all-trans conformation one can see from Figure 20 that the C_3 axis is almost parallel to L in the odd chain (bond type 1) and is inclined to L at nearly the magic angle (bond type 2) in the even numbered chains. A quantitative expression for the methyl splitting in our model must also include the kink probability, P^{n-1} , of the penultimate carbon atom, since this will change the orientation of the C_3 axis (for odd membered chains from type 1 to type 3, and for even chains from type 2 to type 3). Thus for odd membered chains the quadrupole splitting is given by

$$\Delta^{CD_3} = -\frac{1}{3} q \cdot S [(1-P^{n-1}) Y(\theta_q^1) + P^{n-1} Y(\theta_q^3)] \quad (VI.9)$$

and for even chains

$$\Delta^{CD_3} = -\frac{1}{3} q \cdot S [(1-P^{n-1}) Y(\theta_q^2) + P^{n-1} Y(\theta_q^3)] \quad (VI.10)$$

Since we expect P^i to increase with temperature and S to decrease it follows from Eq. (VI.9) that, at least for small P^{n-1} , $|\Delta^{CD_3}|$ for odd chains should be large and decrease with increasing temperature, as is indeed observed in 40·7 and 60·7. The situation for even chains is more complicated because the term in square brackets in Eq. (VI.10) consists of two small numbers that may have the same or opposite sign, depending on the value of α' chosen. For $\alpha' > 17^\circ$ the first term is negative while the second positive and thus a continuous change in P^{n-1} will cause Δ^{CD_3} to pass through zero. This is probably the

origin of the change in sign upon changing of temperatures observed by Deloche and Charvolin¹⁷ in the methyl group of BOBOA, and also the reason for the anomalous temperature dependence of the CD₃ deuterons in 50.7 and 70.7.

The methyl splitting depicted in Figure 19 were calculated from Eqs. (VI.9) and (VI.10) with the same parameters as used to calculate the methylene splitting. The general behavior of these splittings (for $\alpha'=20^\circ$) is again consistent with the results of Figures 16 and 17. Note that in these calculations the sign of Δ^{CD_3} for 50.7 and 70.7 came out opposite to that of the methylene deuterons, while for 40.7 and 60.7 all Δ 's have the same sign.

C. Kink Probabilities.

We now reverse the procedure used above and attempt to estimate the kink probabilities P^1 from the methylene and methyl quadrupole splitting constants. To do that we need to fix two parameters; (i) α' , which determines the various θ 's and (ii) the order parameters. From the discussion in part A of this section we expect α' to be approximately 20° . The value of S is more difficult to determine. It varies from compound to compound and is temperature dependent. The results from the benzyldene deuterons (Figure 14) are not very useful due to the uncertainty in which set of data to choose. From Eq. (VI.1a) we note that fixing the value of S determines uniquely P^2 and vice versa. We preferred to optimize the value of P^2 , because this parameter has a simpler physical meaning. To do this, plots of

the type shown in Figure 19 were calculated by varying P^2 , and to some extent also α' , and compared with the experimental results in Figures 16 and 17 for each compound. The calculations were made with various functions in which the P^i 's were assumed to increase monotonically with i . Examples of such plots for the alkoxy chain of 60·7 are shown in Figure 21. We found that under this restriction good overall fit with the experimental results could only be obtained for $\alpha' \approx 20^\circ$ and P^2 values ranging between zero and 0.1. The final values adopted were

$$P^2 = 0.05 \text{ for } 40\cdot7 \text{ and } 50\cdot7$$

and

$$P^2 = 0.01 \text{ for } 60\cdot7 \text{ and } 70\cdot7$$

With this choice of P^2 and $\alpha' = 20^\circ$, and using the experimental splittings of the methylene deuterons, the results plotted in Figures 22 and 23 for the P^i 's in the various compounds and phases were obtained (full symbols). Values for P^{n-1} could also be calculated from the CD_3 splitting (Eqs. VI.9 and VI.10). In these calculations we assigned positive signs to the methyl splittings in 50·7 and 70·7 while in 40·7 and 60·7 this sign was taken as negative - the same as for all the methylenes. This choice of signs was derived from the best fit analysis described above. The values of P^{n-1} calculated from the methyl group are indicated by open symbols in Figures 22 and 23, they fit pretty well with those derived from methylene splitting.

There is a considerable scatter in the experimental points in these figures, in particular some of the points for odd atoms, e.g., $i=5$ in 50·7 and 60·7, deviate significantly from the general trend. We believe that this results from the sensitivity of P^i for odd kinks

to the parameters used, as compared to even kinks. The difference in sensitivity results from the fact discussed above that an odd kink affects Δ much less than does an even kink (see e.g., Figures 19 and 21). We therefore regard the results for even kinks as more reliable. The continuous lines in Figures 22 and 23, indicating the increase in P^i for the various phases were drawn by considering only the even kinks.

The same type of information, concerning kink probabilities, could in principle be derived from the methylene dipolar interaction, however the dipolar data are much less complete and considerably less accurate. The general behavior of the dipolar splittings is however consistent with the results derived from the quadrupolar splittings. In Table IV are compared experimental dipolar interaction between methylene deuterons (in each case relative to the corresponding $D^{\alpha\alpha}$) with those calculated from Eqs. (VI.3) and (VI.4) using the P^i 's of Figures 22 and 23. The data in each compound are for the smectic A (or B_A) phase for which the spectra are usually best resolved. Considering the uncertainties in the D's and P's the agreement is quite satisfactory.

Of particular interest is the α - γ dipolar interaction obtained in 50•7 by the D.Q. method. For an all trans conformation we would expect the ratio $(D^{\alpha_1\gamma} + D^{\alpha_2\gamma})/D^{\alpha\alpha}$ to be 0.82, while experimentally (see Figure 11) this ratio is considerably smaller, ~ 0.50 . The discrepancy between the two figures can, to a large extent, be accounted for by considering the kinked conformations. Using the results for P^i from Figure 22 we calculate $(D^{\alpha_1\gamma} + D^{\alpha_2\gamma})/D^{\alpha\alpha} = 0.62$ (and $(D^{\alpha_1\gamma} - D^{\alpha_2\gamma})/D^{\alpha\alpha} = 0.15$).

The numerical results for the kink probabilities should of course not be taken too seriously in view of the simple minded model used, and the many assumptions made. However, the similarity between the experimental patterns of the quadrupole and dipolar splitting constants and the calculated ones, suggest that the trend of the P^i 's in Figures 22 and 23 is correct, and that the numerical values are of the right order: perhaps within a factor of 1.5 to two.

There does not seem to be a conspicuous change in the P^i pattern on going from one phase to another. The small increase in P^i on going from the more ordered phases (smectic B) to the less ordered ones (smectic A and nematic) probably reflects the increase in the chain's orientational disorder with increasing temperature. In other words, there does not appear to be a predominant effect of the molecular packing in the various mesophases on the chain conformation.

From the results for P^i one can estimate the kink probability per chain

$$P_k = \sum_i P^i \quad (\text{VI.11})$$

as well as the probability for a gauche conformation per segment.

$$P_g = \frac{2P_k}{n-1} \quad (\text{VI.12})$$

Using the data for Figures 22 and 23, P_k is found to range between ~ 0.5 for 40.7 to ~ 1 for 70.7 , while P_g is found to range between 0.20 and 0.35 depending on the phase and temperature. This corresponds to an average shrinking of the chain length by about 10% from the all trans extended length.

It is interesting to compare the present results for thermotropic liquid crystals with similar data in lyotropic phases. DMR in phospholipids and soaps often show a pattern of quadrupole splitting in which the first two thirds or so of the methylenes have approximately the same Δ 's (plateau), while the splitting of the end methylenes decrease in a manner similar to the characteristic steps reported here.^{22,29-32} By analogy with our discussion above this may be considered as evidence for the occurrence of kinks as the dominant conformational defects in the tail end of the chains, and suggests that the aliphatic chain axis in these mesophases is inclined to the "molecular long axis".

As for comparison with theoretical prediction there is only one work that directly refers to quadrupole splittings of the alkoxy chain, i.e., that of Marcelja.⁵⁷ Unfortunately there is very little similarity between the predicted pattern of the splitting and that actually observed.

ACKNOWLEDGEMENT

We are very grateful to Professor A. Pines for his advice and support and for many illuminating discussions. We also thank David Wemmer and Daniel Weitekamp for assistance with the experiments and for many helpful discussions on Fourier transform double quantum spectroscopy.

APPENDIX A

In this appendix we calculate the single quantum NMR spectrum of spin $I = 1$ nuclei, with both quadrupole and dipolar interactions for three cases: (i) two interacting nuclei, with different quadrupolar interaction (type AB), (ii) three interacting equivalent nuclei with D_3 permutation symmetry (type A_3), and (iii) three interacting nuclei, two of which have identical quadrupolar interaction, but different dipolar interaction with the third nucleus (type $AA'B$). The first case applies to the phenyl deuterons of the benzylidene ring, the second to the methyl deuterons (in general), and the third to a methylene CD_2 group interacting with a third deuteron in the molecule. In all cases we consider only the direct dipolar interaction and neglect the chemical shift and indirect spin-spin decoupling, since for deuterons the latter interactions are negligibly small. In fact for the cases discussed in the text they are considerably smaller than the linewidths. Also we assume an axial quadrupole interaction and use the high field approximation.⁵⁸

(i) We consider two nuclei with quadrupole interactions ν_Q^A, ν_Q^B and direct dipolar interaction $D = D^{AB}$. The spin Hamiltonian is:

$$\mathcal{H} = -\nu_0(I_z^A + I_z^B) + \nu_Q^A(I_z^A)^2 + \nu_Q^B(I_z^B)^2 + D[I_z^A I_z^B - \frac{1}{4}(I_{+-}^A I_{-+}^B + I_{-+}^A I_{+-}^B)] \quad (A1)$$

The basic functions used and their designations are listed below:

$$\phi_2 = (1 \ 1)$$

$$\phi_1^A = (1 \ 0)$$

$$\phi_1^B = (0 \ 1)$$

$$\phi_0^0 = (0 \ 0)$$

$$\phi_0^S = \frac{1}{\sqrt{2}} [(1 \ -1) + (-1 \ 1)]$$

$$\phi_0^a = \frac{1}{\sqrt{2}} [(1 \ -1) - (-1 \ 1)]$$

$$\phi_{-1}^A = (-1 \ 0)$$

$$\phi_{-1}^B = (0 \ -1)$$

$$\phi_{-2} = (-1 \ -1)$$

where the numbers in the parentheses refer to the azimuthal quantum numbers of nuclei A and B respectively. With this basis set, the only off diagonal matrix elements of the Hamiltonian (A1) are between the functions $\phi_{\pm 1}^A$ and $\phi_{\pm 1}^B$ and between ϕ_0^0 and ϕ_0^S . Calculation of the matrix elements and diagonalizing the three 2 x 2 matrices yield the eigenfunctions and eigenvalues given in Table V. In this table the angles β and α are defined by

$$\tan 2\beta = \sqrt{2} D / (v_Q^A + v_Q^B - D) \quad (A2)$$

$$\tan 2\alpha = D / (v_Q^B - v_Q^A) \quad (A3)$$

and the eigenfunctions were labeled such that they become equivalent to those used for the case of two equivalent nuclei when $v_Q^A - v_Q^B \rightarrow 0$.¹² From these results the transition frequencies given in the second column of Table VI are computed. In the present case of the phenyl deuterons, these expressions can be simplified by the following consideration.

Since

$$|D| \ll |v_Q^A + v_Q^B| \quad (A4)$$

(assuming both v_Q^A and v_Q^B have the same sign) we can set

$$\sin\beta = 0 ; \cos\beta = 1 ; \frac{1}{\sqrt{2}} D \cot\beta = \nu_Q^A + \nu_Q^B - D \quad (\text{A5})$$

However since

$$|D| \lesssim |\nu_Q^B - \nu_Q^A| \quad (\text{A6})$$

we calculate the frequencies to second order in $D/(\nu_Q^B - \nu_Q^A)$ and set

$$\frac{1}{2} D \cot\alpha = \nu_Q^B - \nu_Q^A + \varepsilon \quad (\text{A7})$$

where

$$\varepsilon = \left(\frac{1}{2} D\right)^2 / (\nu_Q^B - \nu_Q^A) \quad (\text{A8})$$

The calculated frequencies and corresponding intensities so obtained, are given in the third and fourth column of Table VI respectively. Thus each quadrupole component consists of a triplet at frequencies $\mp D, 0$ and $\pm D$, centered about $\pm(\nu_Q^A - \varepsilon)$ and $\pm(\nu_Q^B + \varepsilon)$, of relative intensities 1, $(\cos\alpha + \sin\alpha)^2$ and $(\cos\alpha - \sin\alpha)^2$, and 1, $(\cos\alpha - \sin\alpha)^2$ and $(\cos\alpha + \sin\alpha)^2$ respectively. A stick diagram of the full spectrum is shown in the upper two trace of Figure 24. The diagram emphasizes the fact that the spectrum is (a) symmetric about ν_0 , and (b) the structure of each quadrupole component is inverted about the corresponding ν_Q upon changing of the relative sign of D to $\nu_Q^B - \nu_Q^A$.

(ii) In this part we calculate the NMR spectrum of three equivalent spin $I = 1$ nuclei with D_3 permutation symmetry. The spin Hamiltonian is:

$$\begin{aligned}
 \mathcal{H} = & -\nu_0 (I_z^1 + I_z^2 + I_z^3) + \nu_Q [(I_z^1)^2 + (I_z^2)^2 + (I_z^3)^2] \\
 & + D(I_z^1 I_z^2 + I_z^1 I_z^3 + I_z^2 I_z^3) - \frac{1}{4} D (I_{+-}^1 I_{-+}^2 + I_{-+}^1 I_{+-}^2 \\
 & + I_{+-}^1 I_{-+}^3 + I_{-+}^1 I_{+-}^3 + I_{+-}^2 I_{-+}^3 + I_{-+}^2 I_{+-}^3) \quad (A9)
 \end{aligned}$$

The basic symmetry functions and the diagonal and off-diagonal element of this Hamiltonian are listed in Table VII. It may be seen that the few off-diagonal terms obtained with this representation are of order D while they connect elements differing by order ν_Q .

In the case treated in this paper, i.e., the CD_3 group, $D \sim 100$ Hz and $\nu_Q \sim 10$ KHz, thus $D \ll \nu_Q$ and we may completely neglect the off-diagonal terms in Table VII. The basis function used and the diagonal matrix elements then become respectively the eigenfunctions and corresponding energies of the problem. The frequencies and transition probabilities obtained in this limit are summarized in Table VIII. These results show that each component of the quadrupole doublet is split into seven lines by the dipolar interaction with relative intensities 3, 8, 3, 1, 7, 3, 2 and frequencies (in units of D) of 3, 1, $\frac{1}{2}$, $-\frac{1}{2}$, -1, -2, $-\frac{5}{2}$ (relative to $\nu_0 + \nu_Q$) respectively. The dipolar structure of the $\nu_0 - \nu_Q$ component is the mirror image (about ν_0) of the $\nu_0 + \nu_Q$ component. As for case (i) the structure of the spectrum depends on the relative signs of D and ν_Q . The middle traces (b) in Figure 24 give stick diagrams of the full spectrum for the two possible signs of D/ν_Q .

(iii) Finally we discuss the spin system $AA'B$, whose spin Hamiltonian is:

$$\begin{aligned}
 \mathcal{H} = & -\nu_0(I_z^A + I_z^{A'} + I_z^B) + \nu_Q^A[(I_z^A)^2 + (I_z^{A'})^2] + \nu_Q^B(I_z^B)^2 \\
 & + D[I_z^A I_z^{A'} - \frac{1}{4}(I_+^A I_-^{A'} + I_-^A I_+^{A'})] + D^{AB}[I_z^A I_z^B - \frac{1}{4}(I_+^A I_-^B + I_-^A I_+^B)] \\
 & D^{A'B}[I_z^{A'} I_z^B - \frac{1}{4}(I_+^{A'} I_-^B + I_-^{A'} I_+^B)] \tag{A10}
 \end{aligned}$$

where $D = D^{AA'}$. We consider the limit in which

$$|D| \ll |\nu_Q^A| \tag{A11}$$

$$|D^{AB}|, |D^{A'B}| \ll |\nu_Q^A - \nu_Q^B| \tag{A12}$$

We can then neglect mixing terms of the type $I_+^A I_+^B$ and $I_-^{A'} I_-^B$ in (A10). The wavefunctions and the energies of the truncated Hamiltonian are summarized in Table IX, and the transition frequencies and intensities in Table X. The resulting spectrum thus consists of two quadrupole doublets each component of which is further split by the dipolar interaction. The dipolar structure of the spectrum depends on the relative magnitudes of D , $SD = D^{AB} + D^{A'B}$ and $RD = D^{AB} - D^{A'B}$. In trace (c) of Figure 24 is shown a stick diagram for half of the AA'B spectrum, using $SD/D = 0.62$ and $RD/D = 0.15$. The parameters were obtained from kink probabilities considerations as discussed in the text. Under these conditions, transition intensities of order $\sin^2 \alpha$ and splittings of order Δ (see Table X) are too small to observe on the scale used.

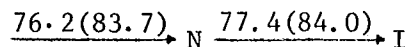
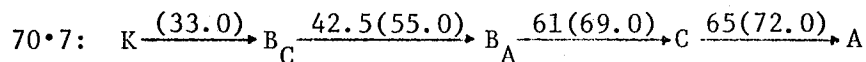
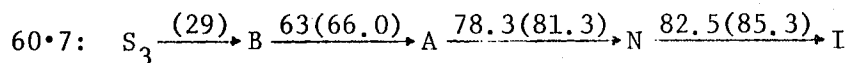
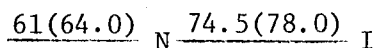
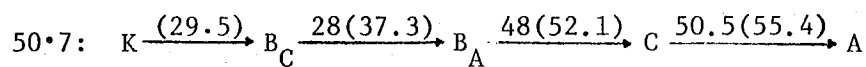
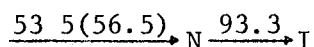
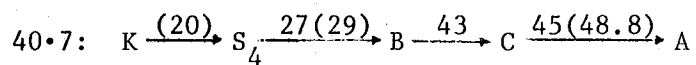
APPENDIX B

We derive the dipolar structure in the D.Q. spectrum for the two cases described in the text, i.e., the A_2 and $AA'B$ systems. The general theory for the dipolar structure in D.Q. spectroscopy will be published elsewhere. Here we merely calculate the spectra of these two cases. The transition frequencies of a particular set of equivalent nuclei (having the same ν_Q) are simple $E^k - E^\ell$ (where ℓ and k label the initial and final states). For the pulse D.Q. experiment the corresponding intensities are proportional to the square of the matrix element of the operator $[\sum_i (I_{\pm}^i)^2]$, where i runs over the set of equivalent nuclei.

(i) The A_2 case: Using the wave functions and energies in Table I of reference 12, four "allowed" D.Q. transitions are obtained. Their frequencies and intensities (in the limit $D \ll \nu_Q$) are given in Table XI. Thus the D.Q. spectrum consists of a symmetric 1:1:1 triplet with spacing $2D$.

(ii) To calculate the D.Q. spectrum of the B deuterons of the $AA'B$ case we use the wave functions and energies for this system given in Table IX. The spectrum is given in Table XII. It consists of a symmetric $1:2 \cos^2 2\alpha:3:2 \cos^2 2\alpha:1$ quintuplet with spacing $SD = (D^{AB} + D^{A'B})$. Each of the $2 \cos^2 2\alpha$ transitions is accompanied by a symmetric doublet of intensity $\sin^2 2\alpha$ and overall splitting $2D - 4\Delta$.

Table I. Phase diagrams and transition temperatures of the normal liquid crystals studied.^{a,b}



^a The letters A, B, C, B_A, B_C refer to the corresponding smectic phases, N is nematic, I is isotropic, and K is crystalline.

^b The numbers above the arrows refer to the transition temperatures in degree celsius; without parentheses - experimental values for the compounds perdeuterated in the alkoxy chains. In parenthesis - literature values^{37,38,41} for the normal compounds.

Table II. Average values for the ratio Δ/D for the end methy CD_3 deuterons in 40 \cdot 7 and 60 \cdot 7.

<u>phase</u>	<u>N</u>	<u>A</u>	<u>C</u>	<u>B</u>
40 \cdot 7	-168 ± 5	-166 ± 5	-172 ± 5	a
60 \cdot 7	a	-170 ± 5	-	-175 ± 10

^a Dipolar structure not sufficiently resolved.

Table III. Formulae and numerical values for θ_q^k , $Y(\theta_q^k)$, θ_d^{kl} , and $Y(\theta_d^{kl})$ for a tetrahedral carbon atom, and various values of α' .

k bond type	General Expression for θ_q^k	$\alpha' = 10^\circ$		$\alpha' = 15^\circ$		$\alpha' = 20^\circ$		$\alpha' = 25^\circ$	
		θ_q^k	$Y(\theta_q^k)$	θ_q^k	$Y(\theta_q^k)$	θ_q^k	$Y(\theta_q^k)$	θ_q^k	$Y(\theta_q^k)$
1	α'	10	+0.955	15	+0.900	20	+0.825	25	+0.732
2	$\pi - \tau - \alpha'$	60.53	-0.137	55.53	-0.020	50.53	+0.106	45.53	+0.236
3,4	$\cos^{-1}[\cos(\frac{\tau}{2} + \alpha') \cos \frac{\tau}{2}]$	75.73	-0.409	78.46	-0.440	81.26	-0.465	84.09	-0.484
kl type of r ^{kl}	for θ_d^{kl}	θ_d^{kl}	$Y(\theta_d^{kl})$	θ_d^{kl}	$Y(\theta_d^{kl})$	θ_d^{kl}	$Y(\theta_d^{kl})$	θ_d^{kl}	$Y(\theta_d^{kl})$
3-4	$\pi/2$	90	-0.500	90	-0.500	90	-0.500	90	-0.500
1-4	$\cos^{-1}[\frac{\sqrt{3}}{2} \sin(\pi - \tau - \alpha')]$	41.07	+0.353	44.44	+0.265	48.05	+0.170	51.83	+0.073
2-3	$\cos^{-1}(\frac{\sqrt{3}}{2} \sin \alpha')$	81.35	-0.466	77.05	-0.425	72.77	-0.368	68.53	-0.299

Table IV. Comparison of the experimental dipolar splittings D^{ii}
(in units of $D^{\alpha\alpha}$) with calculated values.

Compound ^a		$\frac{D^{\beta\beta}}{D^{\alpha\alpha}}$	$\frac{D^{\gamma\gamma}}{D^{\alpha\alpha}}$	$\frac{D^{\delta\delta}}{D^{\alpha\alpha}}$	$\frac{D^{\epsilon\epsilon}}{D^{\alpha\alpha}}$	$\frac{D^{\xi\xi}}{D^{\alpha\alpha}}$
40·7	exp.	0.94	___ b			
(A, 50)	calc.	0.91	0.62			
50·7	exp.	0.97	___ b	___ b		
(A, 56)	calc.	0.91	0.70	0.70		
60·7	exp.	1	0.7	0.7	___ b	
(A, 70)	calc.	0.98	0.77	0.73	0.53	
70·7	exp.	1	0.8	0.8	0.6	0.6
(B _A , 55)	calc.	0.98	0.89	0.87	0.78	0.76

^a Under the compounds name are given the phase and temperature for which the calculations were done.

^b Dipolar structure not resolved.

Table V. Eigenfunctions and energies for the Hamiltonian (A1).

M_I	eigenfunction	energies
2	ϕ_2	$-2v_0 + v_Q^A + v_Q^B + D$
1	$\phi_1^s = \cos\alpha \phi_1^A + \sin\alpha \phi_1^B$	$-v_0 + v_Q^B - \frac{1}{2} D \cot\alpha$
1	$\phi_1^a = \sin\alpha \phi_1^A - \cos\alpha \phi_1^B$	$-v_0 + v_Q^A + \frac{1}{2} D \cot\alpha$
0	$\phi_0^{s1} = \cos\beta \phi_0^A + \sin\beta \phi_0^B$	$v_Q^A + v_Q^B - D(1 + \frac{1}{\sqrt{2}} \cot\beta)$
0	$\phi_0^{s2} = \sin\beta \phi_0^A - \cos\beta \phi_0^B$	$\frac{1}{\sqrt{2}} D \cot\beta$
0	ϕ_0^a	$v_Q^A + v_Q^B - D$
-1	$\phi_{-1}^s = \cos\alpha \phi_{-1}^A + \sin\alpha \phi_{-1}^B$	$v_0 + v_Q^B - \frac{1}{2} D \cot\alpha$
-1	$\phi_{-1}^a = \sin\alpha \phi_{-1}^A - \cos\alpha \phi_{-1}^B$	$v_0 + v_Q^A + \frac{1}{2} D \cot\alpha$
-2	ϕ_{-2}	$2v_0 + v_Q^A + v_Q^B + D$

Table VI. Transition frequencies and intensities for the two deuteron case.^a

<u>Transition</u>	<u>Frequency</u> ^b	<u>Frequency</u> ^c	<u>Intensity</u>
$\phi_1^a \leftarrow \phi_2$	$\nu_0 - \nu_Q^B - D(1 - \frac{1}{2} \cot\alpha)$	$\nu_0 - \nu_Q^A - D + \epsilon$	$2(\cos\alpha - \sin\alpha)^2$
$\phi_0^{s1} \leftarrow \phi_1^s$	$\nu_0 + \nu_Q^A - D(1 - \frac{1}{2} \cot\alpha + \frac{1}{\sqrt{2}} \cot\beta)$	$\nu_0 - \nu_Q^A + \epsilon$	$2(\cos\alpha + \sin\alpha)^2$
$\phi_{-1}^a \leftarrow \phi_0^{s2}$	$\nu_0 + \nu_Q^A + D(\frac{1}{2} \cot\alpha - \frac{1}{\sqrt{2}} \cot\beta)$	$\nu_0 - \nu_Q^A + D + \epsilon$	$(\cos\alpha - \sin\alpha)^2$
$\phi_{-1}^a \leftarrow \phi_0^a$	$\nu_0 - \nu_Q^B + D(1 + \frac{1}{2} \cot\alpha)$		$(\cos\alpha + \sin\alpha)^2$
$\phi_1^s \leftarrow \phi_2$	$\nu_0 - \nu_Q^A - D(1 + \frac{1}{2} \cot\alpha)$	$\nu_0 - \nu_Q^B - D - \epsilon$	$2(\cos\alpha + \sin\alpha)^2$
$\phi_0^{s1} \leftarrow \phi_1^a$	$\nu_0 + \nu_Q^B - D(1 - \frac{1}{2} \cot\alpha + \frac{1}{\sqrt{2}} \cot\beta)$	$\nu_0 - \nu_Q^B - \epsilon$	$2(\cos\alpha - \sin\alpha)^2$
$\phi_{-1}^s \leftarrow \phi_0^{s2}$	$\nu_0 + \nu_Q^B - D(\frac{1}{2} \cot\alpha + \frac{1}{\sqrt{2}} \cot\beta)$	$\nu_0 - \nu_Q^B + D - \epsilon$	$(\cos\alpha + \sin\alpha)^2$
$\phi_{-1}^s \leftarrow \phi_0^a$	$\nu_0 - \nu_Q^A + D(1 - \frac{1}{2} \cot\alpha)$		$(\cos\alpha - \sin\alpha)^2$

^a Only the high frequency half of the spectrum is given (assuming $\nu_Q^A, \nu_Q^B > 0$).

The low frequency half is symmetric about ν_0 ; the transition $\phi_{-j} \rightarrow \phi_{-i}$ corresponding to the negative (about ν_0) of the transition $\phi_i \rightarrow \phi_j$.

^b Exact result.

^c Transition frequencies under conditions (A4) and (A6).

Table VII. Symmetry basis functions for three spin $I = 1$ nuclei forming a D_3 permutation group and the corresponding matrix elements of the Hamiltonian (A9).

M_I	<u>Class A wavefunctions^a</u>	<u>diagonal</u>	<u>off-diagonal^b</u>
1	3 (111)	$-3v_0 + 3v_Q + 3D$	
2	$3^{-\frac{1}{2}}[(110) + (101) + (011)]$	$-2v_0 + 2v_Q$	
3	$3^{-\frac{1}{2}}[(100) + (010) + (001)]$	$-v_0 + v_Q - D$	} - D
4	$3^{-\frac{1}{2}}[(11-1) + (1-11) + (-111)]$	$-v_0 + 3v_Q - D$	
5	0 (000)	0	} $-\sqrt{\frac{3}{2}} D$
6	$6^{-\frac{1}{2}}[(01-1) + (-101) + (1-10)$ $+ (0-11) + (10-1) + (-110)]$	$2v_Q - 2D$	
7	$6^{-\frac{1}{2}}[(01-1) + (-101) + (1-10)$ $- (0-11) - (10-1) - (-110)]$	$2v_Q$	
<u>Class E wavefunctions</u>			
8	$2^{-\frac{1}{2}}[(101) - (011)]$	$-2v_0 + 2v_Q + \frac{3}{2} D$	
9	$6^{-\frac{1}{2}}[2(110) - (101) - (011)]$	$-2v_0 + 2v_Q + \frac{3}{2} D$	
10	$2^{-\frac{1}{2}}[(100) - (010)]$	$-v_0 + v_Q + \frac{1}{2} D$	} $-\frac{1}{2} D$
11	$2^{-\frac{1}{2}}[(1-11) - (-111)]$	$-v_0 + 3v_Q - D$	
12	$6^{-\frac{1}{2}}[2(001) - (100) - (010)]$	$-v_0 + v_Q + \frac{1}{2} D$	} $+\frac{1}{2} D$
13	$6^{-\frac{1}{2}}[2(11-1) - (1-11) - (-111)]$	$-v_0 + 3v_Q - D$	
14	$\frac{1}{2}[(1-10) - (01-1) + (0-11) - (-110)]$	$2v_Q - \frac{3}{2} D$	
15	$12^{-\frac{1}{2}}[2(-101) - (1-10) - (01-1)$ $-2(10-1) + (0-11) + (-110)]$	$2v_Q - \frac{3}{2} D$	
16	$\frac{1}{2}[(1-10) - (01-1) - (0-11) + (-110)]$	$2v_Q - \frac{1}{2} D$	
17	$12^{-\frac{1}{2}}[2(-101) - (1-10) - (01-1)$ $+2(10-1) - (0-11) - (-110)]$	$2v_Q - \frac{1}{2} D$	

Table VII continued.

^a Only the wavefunctions for $M_I \geq 0$ are given. The wavefunctions for negative M_I 's are obtained from the corresponding positive M_I wavefunctions by interchanging the m_I states 1 by -1 and vice versa. The matrix elements for the negative M_I wavefunction are the same as the corresponding positive M_I wavefunction except for a change of sign in the coefficient of v_0 .

^b The off-diagonal element connect the elements indicated by the curly parentheses.

Table VIII. Transition frequencies and intensities for the three spin

I = 1 case, with D_3 symmetry (for $D \ll \nu_Q$).^a

Class A transitions

<u>Transition</u>	<u>Frequency</u>	<u>Intensity</u>
2 ← 1	$\nu_0 - \nu_Q - 3D$	3
3 ← 2	$\nu_0 - \nu_Q - D$	4
4 ← 2	$\nu_0 + \nu_Q - D$	1
5 ← 3	$\nu_0 - \nu_Q + D$	3
6 ← 3	$\nu_0 + \nu_Q - D$	2
6 ← 4	$\nu_0 - \nu_Q - D$	2

Class E transitions

10,12 ← 8,9	$\nu_0 - \nu_Q - D$	2
11,13 ← 8,9	$\nu_0 + \nu_Q - \frac{5}{2} D$	2
14,15 ← 10,12	$\nu_0 + \nu_Q - 2D$	3
16,17 ← 10,12	$\nu_0 + \nu_Q - D$	1
14,15 ← 11,13	$\nu_0 - \nu_Q - \frac{1}{2} D$	3
16,17 ← 11,13	$\nu_0 - \nu_Q + \frac{1}{2} D$	1

^a Only half the transitions are given. The frequencies of the other transitions are obtained from those in the Table by inverting the signs of the coefficients of ν_Q and D . The corresponding intensities are the same.

Table IX. Wavefunctions and energies for the AA'B case under conditions A(11) and A(12).^a

M_I	Wavefunction	Energy
3	$\phi_3 = (111)$	$-3v_0 + 2v_Q^A + v_Q^B + D + SD$
2	$\phi_2^1 = (110)$	$-2v_0 + 2v_Q^A + D$
2	$\phi_2^2 = 2^{-\frac{1}{2}}\cos\alpha[(011)+(101)] + 2^{-\frac{1}{2}}\sin\alpha[(011)-(101)]$	$-2v_0 + v_Q^A + v_Q^B + \frac{1}{2}SD + \frac{1}{2}D - \frac{1}{2}RD \cot\alpha$
2	$\phi_2^3 = 2^{-\frac{1}{2}}\sin\alpha[(011)+(101)] - 2^{-\frac{1}{2}}\cos\alpha[(011)-(101)]$	$-2v_0 + v_Q^A + v_Q^B + \frac{1}{2}SD - \frac{1}{2}D + \frac{1}{2}RD \cot\alpha$
1	$\phi_1^1 = (001)$	$-v_0 + v_Q^B$
1	$\phi_1^2 = 2^{-\frac{1}{2}}[(100)+(010)]$	$-v_0 + v_Q^A - \frac{1}{2}D$
1	$\phi_1^3 = 2^{-\frac{1}{2}}[(100)-(010)]$	$-v_0 + v_Q^A + \frac{1}{2}D$
1	$\phi_1^4 = (11-1)$	$-v_0 + 2v_Q^A + v_Q^B + D - SD$
1	$\phi_1^5 = (1-11)$	$-v_0 + 2v_Q^A + v_Q^B - D + RD$
1	$\phi_1^6 = (-111)$	$-v_0 + 2v_Q^A + v_Q^B - D - RD$
0	$\phi_0^1 = 2^{-\frac{1}{2}}\cos\alpha[(10-1)+(01-1)] + 2^{-\frac{1}{2}}\sin\alpha[(10-1)-(01-1)]$	$v_Q^A + v_Q^B - \frac{1}{2}SD + \frac{1}{2}D - \frac{1}{2}RD \cot\alpha$
0	$\phi_0^2 = 2^{-\frac{1}{2}}\sin\alpha[(10-1)+(01-1)] - 2^{-\frac{1}{2}}\cos\alpha[(10-1)-(01-1)]$	$v_Q^A + v_Q^B - \frac{1}{2}SD - \frac{1}{2}D + \frac{1}{2}RD \cot\alpha$
0	$\phi_0^3 = 2^{-\frac{1}{2}}\cos\alpha[(-101)+(0-11)] + 2^{-\frac{1}{2}}\sin\alpha[(-101)-(0-11)]$	$v_Q^A + v_Q^B - \frac{1}{2}SD + \frac{1}{2}D - \frac{1}{2}RD \cot\alpha$
0	$\phi_0^4 = 2^{-\frac{1}{2}}\sin\alpha[(-101)+(0-11)] - 2^{-\frac{1}{2}}\cos\alpha[(-101)-(0-11)]$	$v_Q^A + v_Q^B - \frac{1}{2}SD - \frac{1}{2}D + \frac{1}{2}RD \cot\alpha$
0	$\phi_0^5 = (1-10)$	$2v_Q^A - D$

Table IX. Continued

0	$\phi_0^6 = (-110)$	$2v_Q^A - D$
0	$\phi_0^7 = (000)$	0

^aOnly wave functions for $M_I \geq 0$ are given in the Table. The following definitions are used:

$$SD = D^{AB} + D^{A'B}; \quad RD = D^{AB} - D^{A'B}; \quad \tan 2\alpha = RD/D.$$

Table X. Transition frequencies and intensities for the S.Q. spectrum of AA'B. ^{a,b}

<u>Transition</u>	<u>Frequency</u>	<u>Intensity</u>
$\phi_3 \rightarrow \phi_2^2$	$\nu_0 - \nu_Q^A - \frac{3}{2} D - \frac{1}{2} SD + \Delta$	$4 \cos^2 \alpha$
$\phi_4 \rightarrow \phi_0^1$	$\nu_0 - \nu_Q^A - \frac{3}{2} D + \frac{1}{2} SD + \Delta$	$4 \cos^2 \alpha$
$\phi_2^1 \rightarrow \phi_1^2$	$\nu_0 - \nu_Q^A - \frac{3}{2} D$	4
$\phi_5 \rightarrow \phi_0^4$	$\nu_0 - \nu_Q^A + \frac{3}{2} D - \frac{1}{2} SD - RD - \Delta$	$1 + \sin 2\alpha$
$\phi_6 \rightarrow \phi_0^4$	$\nu_0 - \nu_Q^A + \frac{3}{2} D - \frac{1}{2} SD + RD - \Delta$	$1 - \sin 2\alpha$
$\phi_3 \rightarrow \phi_1^5$	$\nu_0 - \nu_Q^A + \frac{3}{2} D + \frac{1}{2} SD - RD - \Delta$	$1 + \sin 2\alpha$
$\phi_3 \rightarrow \phi_1^6$	$\nu_0 - \nu_Q^A + \frac{3}{2} D + \frac{1}{2} SD + RD - \Delta$	$1 - \sin 2\alpha$
$\phi_3 \rightarrow \phi_0^6$	$\nu_0 - \nu_Q + \frac{3}{2} D$	2
$\phi_3 \rightarrow \phi_0^5$		
$\phi_2^2 \rightarrow \phi_1^1$	$\nu_0 - \nu_Q^A + \frac{1}{2} D - \frac{1}{2} SD - \Delta$	$4 \cos^2 \alpha$
$\phi_1^1 \rightarrow \phi_0^3$	$\nu_0 - \nu_Q^A + \frac{1}{2} D + \frac{1}{2} SD - \Delta$	$4 \cos^2 \alpha$
$\phi_6 \rightarrow \phi_0^3$	$\nu_0 - \nu_Q^A + \frac{1}{2} D - \frac{1}{2} SD + RD + \Delta$	$1 + \sin 2\alpha$
$\phi_6 \rightarrow \phi_0^4$	$\nu_0 - \nu_Q^A + \frac{1}{2} D - \frac{1}{2} SD - RD + \Delta$	$1 - \sin 2\alpha$
$\phi_2^2 \rightarrow \phi_1^5$	$\nu_0 - \nu_Q^A + \frac{1}{2} D + \frac{1}{2} SD - RD + \Delta$	$1 - \sin 2\alpha$
$\phi_2^2 \rightarrow \phi_1^6$	$\nu_0 - \nu_Q^A + \frac{1}{2} D + \frac{1}{2} SD + RD + \Delta$	$1 + \sin 2\alpha$
$\phi_2^2 \rightarrow \phi_0^7$	$\nu_0 - \nu_Q^A + \frac{D}{2}$	6
$\phi_2^2 \rightarrow \phi_0^6$		
$\phi_2^2 \rightarrow \phi_0^5$		

Table X. Continued

$\phi_3 \rightarrow \phi_2^3$	$\nu_0 - \nu_Q^A - \frac{D}{2} - \frac{1}{2} SD - \Delta$	$4 \sin^2 \alpha$
$\phi_2^3 \rightarrow \phi_1^1$	$\nu_0 - \nu_Q^A - \frac{D}{2} + \frac{1}{2} SD + \Delta$	$4 \sin^2 \alpha$
$\phi_1^1 \rightarrow \phi_0^4$	$\nu_0 - \nu_Q^A - \frac{D}{2} + \frac{1}{2} SD + \Delta$	$4 \sin^2 \alpha$
$\phi_1^4 \rightarrow \phi_0^2$	$\nu_0 - \nu_Q^A - \frac{D}{2} + \frac{1}{2} SD - \Delta$	$4 \sin^2 \alpha$

Transitions of the B nucleus

<u>Transition</u>	<u>Frequency</u>	<u>Intensity</u>
$\phi_3 \rightarrow \phi_2^1$	$\nu_0 - \nu_Q^B - SD$	2
$\phi_2^1 \rightarrow \phi_1^4$	$\nu_0 - \nu_Q^B + SD$	2
$\phi_2^2 \rightarrow \phi_1^2$	$\nu_0 - \nu_Q^B - \frac{1}{2} SD - \Delta$	$2 \cos^2 \alpha$
$\phi_2^3 \rightarrow \phi_1^3$	$\nu_0 - \nu_Q^B - \frac{1}{2} SD + \Delta$	$2 \cos^2 \alpha$
$\phi_1^2 \rightarrow \phi_0^1$	$\nu_0 - \nu_Q^B + \frac{1}{2} SD - \Delta$	$2 \cos^2 \alpha$
$\phi_1^3 \rightarrow \phi_0^2$	$\nu_0 - \nu_Q^B + \frac{1}{2} SD + \Delta$	$2 \cos^2 \alpha$
$\phi_1^1 \rightarrow \phi_0^7$	$\nu_0 - \nu_Q^B$	2
$\phi_1^6 \rightarrow \phi_0^6$	$\nu_0 - \nu_Q^B + RD$	2
$\phi_1^5 \rightarrow \phi_0^5$	$\nu_0 - \nu_Q^B - RD$	2
$\phi_2^3 \rightarrow \phi_1^2$	$\nu_0 - \nu_Q^B - D - \frac{1}{2} SD + \Delta$	$2 \sin^2 \alpha$

Table X. Continued

$\phi_1^2 \rightarrow \phi_0^2$	$\nu_0 - \nu_Q^B - D + \frac{1}{2} SD + \Delta$	$2 \sin^2 \alpha$
$\phi_2^2 \rightarrow \phi_1^3$	$\nu_0 - \nu_Q^B + D - \frac{1}{2} SD - \Delta$	$2 \sin^2 \alpha$
$\phi_1^3 \rightarrow \phi_0^1$	$\nu_0 - \nu_Q^B + D + \frac{1}{2} SD - \Delta$	$2 \sin^2 \alpha$

^a Only the transition of one component for each of the quadrupole doublets are given. The whole spectrum is symmetric about ν_0 .

^b The symbols are as defined in Table IX and $\Delta = D - \frac{1}{2} RD \cot \alpha$

Table XI. Transition frequencies and intensities for the D.Q. spectrum of the A_2 system (in the limit $D \ll \nu_q$).

<u>Transition</u> ^a	<u>Frequency</u>	<u>Intensity</u> ^b
$\phi_2^{S1} \leftarrow \phi_2^S$	$2\nu_0 - 2D$	8
$\phi_{-1}^S \leftarrow \phi_1^S$	$2\nu_0$	4
$\phi_{-1}^a \leftarrow \phi_1^a$	$2\nu_0$	4
$\phi_{-2}^S \leftarrow \phi_0^{S1}$	$2\nu_0 + 2D$	8

^a The wave functions are defined as in reference 12;

$$\phi_2^S = (11) ; \phi_1^S = 2^{-\frac{1}{2}}[(10) + (01)] ; \phi_0^{S1} = 2^{-\frac{1}{2}}[(1-1) + (-11)]$$

$$\phi_1^a = 2^{-\frac{1}{2}}[(10) - (01)]$$

^b Calculated from $\{ \langle \phi^k | [(I_{-1}^A)^2 + (I_{-2}^A)^2] | \phi^l \rangle \}^2$, where ϕ^l and ϕ^k are the initial and final states.

Table XII. Transition frequencies and intensities for the B nucleus
in the D.Q. spectrum of AA'B.^a

<u>Transition</u>	<u>Frequency</u>	<u>Intensity</u>
$\phi_3 \rightarrow \phi_1^4$	$2\nu_0 - 2SD$	1
$\phi_2^2 \rightarrow \phi_0^1$	$2\nu_0 - SD$	$2 \cos^2 2\alpha$
$\phi_2^3 \rightarrow \phi_0^2$		
$\phi_1^1 \rightarrow \phi_{-1}^1$	$2\nu_0$	3
$\phi_1^5 \rightarrow \phi_{-1}^5$		
$\phi_1^6 \rightarrow \phi_{-1}^6$		
$\phi_0^2 \rightarrow \phi_{-2}^3$	$2\nu_0 + SD$	$2 \cos^2 2\alpha$
$\phi_0^1 \rightarrow \phi_{-2}^2$		
$\phi_{-1}^4 \rightarrow \phi_{-3}^4$	$2\nu_0 + 2SD$	1
$\phi_2^2 \rightarrow \phi_0^2$	$2\nu_0 - SD + D - 2\Delta$	$\sin^2 2\alpha$
$\phi_2^3 \rightarrow \phi_0^1$	$2\nu_0 - SD - D + 2\Delta$	$\sin^2 2\alpha$
$\phi_0^2 \rightarrow \phi_{-2}^2$	$2\nu_0 + SD - D + 2\Delta$	$\sin^2 2\alpha$
$\phi_0^1 \rightarrow \phi_{-2}^3$	$2\nu_0 + SD + D - 2\Delta$	$\sin^2 2\alpha$

^a The symbols are as defined in Tables IX and X.

REFERENCES

* Research supported by the U.S. Energy Research and Development Administration, Division of Physical Research.

† On Sabattical leave from the Iostope Division, Weizmann Institute of Science, Rehovot, Israel.

1. R.D. Spence, H.S. Gutowsky and C.H. Holm, J. Chem. Phys. 21, 1891 (1953).
2. K.H. Weber, Ann. Physik 3, 1 (1959).
3. Z. Luz and S. Meiboom, J. Chem. Phys. 59, 275 (1973).
4. R.A. Wise, D.H. Smith and J.W. Doane, Phys. Rev. A7, 1366 (1973).
5. S.K. Ghosh, Solid State Comm. 11, 1763 (1972).
6. J.J. Visintainer, E. Bock, R.Y. Dong and E. Tomchuk, Can. J. Phys. 53, 1483 (1975).
7. N. Brown, J.W. Doane, S.L. Arona and J.L. Ferguson, J. Chem. Phys. 50, 1398 (1969).
8. A. Pines and J.J. Chang, Phys. Rev. A10, 946 (1974).
9. A. Pines, D.J. Ruben and S. Allison, Phys. Rev. Lett. 33, 1002 (1974).
10. J.W. Emsley and J.C. Lindon, "NMR Spectroscopy Using Liquid Crystal Solvents" Pergamon Press, 1975, Chapter 6.
11. J.C. Rowell, W.D. Phillips, L.R. Melby and R. Panar, J. Chem. Phys. 43, 3442 (1965).
12. Z. Luz, R.C. Hewitt and S. Meiboom, J. Chem. Phys. 61, 1758 (1974).
13. P. Diehl and A.S. Tracey, Molec. Phys. 30, 1917 (1975).
14. J.W. Emsley, J.C. Lindon and G.R. Luckhurst, Molec. Phys. 30, 1913 (1975).

15. B. Deloche, J. Charvolin, L. Liebert and L. Strzelecki, J. Phys. 36, C1-21 (1975).
16. J. Charvolin and B. Deloche, J. Phys. 37, C3-69 (1976).
17. B. Deloche and J. Charvolin, J. Phys. 37, 1497 (1976).
18. Y.S. Lee, Y.Y. Hsu and D. Dolphin, in "Liquid Crystals and Ordered Fluids" Vol. 2, edited by J.F. Johnson and R.S. Porter (Plenum, New York, 1974) p. 357.
19. R.Y. Dong, E. Tomchuk, C.E. Wade, J.J. Visintainer and E. Bock, J. Chem. Phys. 66, 4121 (1977).
20. E. Oldfield, D. Chapman and W. Derbyshire, FEBS Letters, 16, 102 (1971).
21. J. Charvolin, P. Manneville and B. Deloche, Chem. Phys. Letters 23, 345 (1973).
22. B. Mely, J. Charvolin and P. Keller, Chem. Phys. Lipids 15, 161 (1975).
23. J. Charvolin and B. Mely in "Magnetic Resonance in Colloid and Interface Science" editors H.A. Resing and C.G. Wade, ACS Symposium series, Vol. 34 (American Chemical Society, Washington, D.C., 1976) p. 48.
24. J. Seelig and W. Niederberger, J. Amer. Chem. Soc. 96, 2069 (1974).
25. J. Seelig and W. Niederberger, Biochem. 13, 1585 (1974).
26. A. Seelig and J. Seelig, Biochem. 13, 4839 (1974).
27. H. Schindler and J. Seelig, Biochem. 14, 2283 (1975).
28. J. Seelig and A. Seelig, Biochem. Biophys. Res. Comm. 57, 406 (1974).
29. J.H. Davis, K.R. Jeffrey, M. Bloom and M.I. Valic in "Magnetic Resonance in Colloid and Interface Science" editors H.A. Resing and C.G. Wade, ACS Symposium series, Vol. 34 (American Chemical Society, Washington, D.C., 1976) p. 70.

30. T.P. Higgs and A.L. MacKay, Chem. Phys. Lipids 20, 105 (1977).
31. K. Abdolall, E.E. Burnell, and M.I. Valic, Chem. Phys. Lipids 20, 115 (1977).
32. J.H. Davis and K.R. Jeffrey, Chem. Phys. Lipids 20, 87 (1977).
33. L.W. Reeve and A.S. Tracey, J. Amer. Chem. Soc. 97, 5729 (1975).
34. F.Y. Fujiwara and L.W. Tracey, J. Amer. Chem. Soc. 98, 6790 (1976).
35. G.W. Stockton, C.F. Polnaszek, A.P. Tulloch, F. Hasan and I.C.P. Smith, Biochem. 15, 954 (1976).
36. H.H. Mantsch, H. Saito and I.C.P. Smith, in "Progress in Nuclear Magnetic Resonance Spectroscopy", editors J.W. Emsley, J. Feeney and L.H. Sutcliffe, Pergamon Press (in press).
37. G.W. Smith and Z.G. Gardlund, J. Chem. Phys. 59, 3214 (1973).
38. Z.G. Gardlund, R.J. Curtis and G.W. Smith in "Liquid Crystals and Ordered Fluids", J.F. Johnson and R.S. Porter, Plenum Press, New York (1974), p. 541, Volume 2.
39. M. Sarai, T. Nakamura and S. Seki, Pramana Suppl. No. 1, 503 (1975) [Chem. Abst. 84, 1144762 (1976)].
40. G.W. Smith, Molec. Cryst. Liq. Cryst. (Letters), 34, 87 (1976).
41. J. Doucet and A.M. Levelut, J. Phys. 38, 1163 (1977).
42. W.H. De Jeu and J.A. De Pooter, Phys. Letters 61A, 114 (1977).
43. S. Vega, T.W. Shattuck, and A. Pines, Phys. Rev. Lett. 37, 43 (1976).
44. S. Vega and A. Pines, J. Chem. Phys. 66, 5624 (1977).
45. D.E. Wemmer, S. Vega, S. Hsi and H. Zimmermann, Poster I-15, Experimental 18th NMR Conference, Asilomar, April, 1977.

46. T.R. Criswell, B.H. Klanderma and D.C. Batesky, Molec. Cryst. Liq. Cryst. 22, 211 (1973).
47. R.E. Partch, Tetrahedron Letters 41, 3071 (1964).
48. H. Gross and G. Matthey, Chem. Ber. 97, 2606 (1964).
49. R.F. Nystrom and W.G. Brown, J. Amer. Chem. Soc. 69, 1197 (1947).
50. Org. Synthesis Coll., Vol. 2, 358 (1943).
51. J.G. Atkinson, J.J. Csakvary, G.T. Herbert and R.S. Stuart, J. Amer. Chem. Soc. 90, 498 (1968).
52. A. Vogel, Practical Organic Chemistry, 3rd ed., (1964), p. 485.
53. D. Wemmer, D. Ruben and A. Pines (to be published).
54. N.O. Petersen and S.I. Chan, Biochem. 16, 2657 (1977).
55. J. Charvolin, Adv. Chem. Series 152, 101 (1976).
56. See for example in "Tables of Interatomic Distances and Configurations of Molecules and Ions" edited by L.E. Sutton (special publication No. 18, The Chemical Society, London, 1965).
57. S. Marcelja, J. Chem. Phys 60, 3599 (1974).
58. Dipolar structure for spin $I = 1$ was also calculated by Emsley and Lindon¹⁰ (see also reference 59). However, in their final results for the A_2 and A_3 cases (in the limit $J \rightarrow 0$ and $D \ll \nu_Q$) numerical errors slipped-in, resulting in incorrect prediction for the spectral structure. The correct spectra are given in references 12 and 60 respectively. We repeat the analysis of the A_3 case because the details of the wave functions and energies are not given in reference 60. The AB case including the indirect spin-spin coupling

and the chemical shift was also treated in reference 10. In this case the line positions and intensities cannot all be given by analytical expressions, and numerical calculations are required in order to obtain the spectrum. Example of such calculated spectra are given in reference 10.

59. J.W. Emsley, J.C. Lindon and J. Tabony, *Molec. Phys.* 26, 1499 (1973).
60. P. Diehl, M. Reinhold and A.S. Tracey, *J. Mag. Res.* 19, 405 (1975).

FIGURE CAPTIONS

1. Deuterium magnetic resonance spectra of the no.7 compounds, perdeuterated in their alkoxy chains, in the isotropic phase. The compounds were contained in the same sample holders, and the spectra recorded under the same conditions (i.e., proton decoupling and without spinning) as used for recording the liquid crystalline phases. The temperature in degrees celsius is given under the compounds name.
2. Proton decoupled deuterium NMR spectra of the four no.7 compounds studied in the mesomorphic state. The temperatures in degrees celsius are given in parentheses under the compound's name. All compounds were perdeuterated in the alkoxy chains. The greek letters refer to the position of the methylene group in the alkoxy chain. The spectra were obtained by Fourier transform of the FID signal following 90° pulses. About 30 to 100 FID signals were accumulated to improve the signal to noise ratio.
3. DMR spectra as in Figure 2 for various isotopic species of 50.7. Only the high field half of the spectrum is shown. All spectra were recorded at 57°C corresponding to the smectic A phase. The first spectrum is of a compound in which the β -protons were randomly exchanged with deuterium to the extent of 15%, while the α -protons were completely substituted by deuterium. The composition given above this trace is the calculated concentration of the major isotopic species. The third and fourth spectra are each of a

mixture of two species as indicated in the figure. The second spectrum is of a single isotopic species as indicated. Note the change in gain in recording the methyl resonance in the third trace.

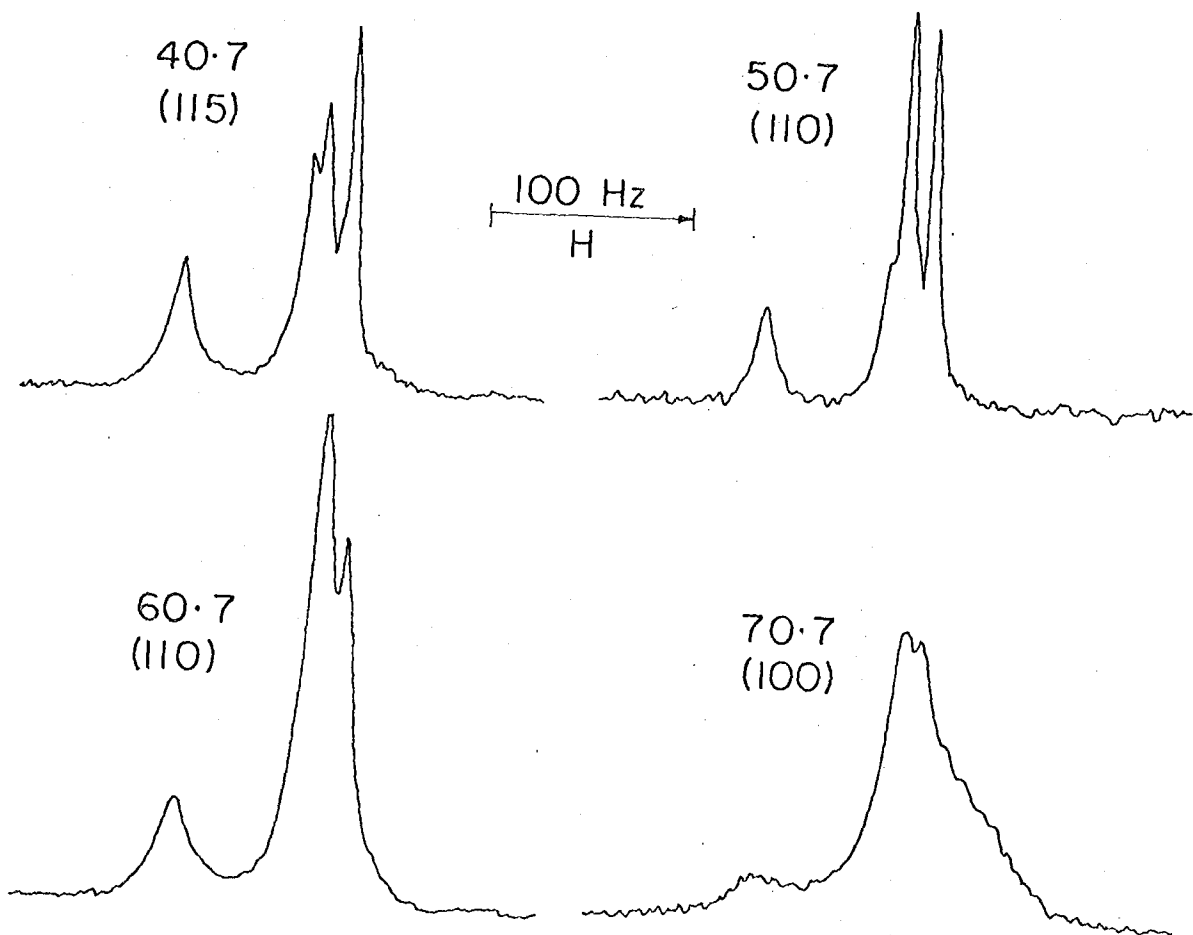
4. Expanded traces of parts of the spectra shown in Figures 2 and 3 to emphasize the structure due to dipolar interaction. Traces a, b, and c show the α and β regions of the first three traces in Figure 3. Traces d and e correspond to the methine and aromatic deuterons of methine- d_1 and benzylidene- d_4 -50.7. Trace f is the methyl resonance in 40.7 perdeuterated in the alkoxy chain, at 47°C. Note that the scale of this trace is twice that of the other traces. The stick diagrams are theoretical and were calculated as explained in the text.
5. Single quantum (left) and double quantum (right) spectra for; (a) the α signal of α_2 - d_2 -50.7 (at 57°C); (b) and (c) the γ signal in $\alpha_2\gamma_1$ - d_3 -50.7 at 57°C and 41°C respectively. Note the different scale used for the two compounds. The stick diagrams give the corresponding theoretical spectra. For $\alpha_2\gamma_1$ - d_3 -50.7 the parameters used are as specified in Figure 24(c).
6. Proton decoupled deuterium magnetic resonance spectra of 40.7 perdeuterated in the alkoxy chain. Only the high field parts of the spectra, one spectrum for each mesophase, are shown. The numbers in parenthesis indicate the temperature in degrees celsius, and the letters refer to the mesophase as in Table I.
7. Same as Figure 6 for 50.7. Note the change in gain for the methyl resonances.
8. Same as Figure 6 for 60.7 (the full spectrum is given in this figure).

9. Same as Figure 6 for 70°7. The nematic phase which is only stable over a very narrow temperature range is always accompanied with some smectic A. The signals due to the smectic A phase in the bottom trace are labeled. The other signals in this trace are due to the nematic phase.
10. Plots of the full quadrupolar splitting $\Delta = 2\nu_Q$, and dipolar interaction D, for the various deuterons in 40°7, as function of temperature. Only the magnitude of the interaction is given--the sign of D/ Δ is negative for both methylene and methyl interactions.
11. Same as in Figure 10 for the various deuterium nuclei of 50°7. The sign of D/ Δ for the phenyl deuterons is positive. The dipolar interaction labeled α - γ refer to the sum of the interactions $D_1^{\alpha,\gamma} + D_2^{\alpha,\gamma}$ obtained by double quantum spectroscopy. Note the change in gain for the CD₃ splitting.
12. Same as in Figure 10 for 60°7.
13. As in Figure 10 for 70°7.
14. Calculated values of α (the angle between the "long molecular axis" and the aromatic ring para axis), and the order parameter S as function of temperature for 50°7 using two sets of data as indicated.
15. Conformation diagrams for the all trans, even kink and odd kink of an eight membered alkoxy chain. The full lines represent bonds in the figure's plane, the short dashed and bold face lines represent C-D bonds in and out of the plane respectively. The heavy lines in the kink structures also represent bonds out of

the figure's plane. The numbers in parentheses refer to type of bonds as discussed in the text. The two long dashed lines are drawn parallel to the molecular long axis.

16. The full points connected by the full lines represent experimental quadrupolar splitting of the deuterons as function of position along the chain at selected temperatures in the various mesophases of 40·7 and 50·7. The temperatures are given in parentheses under the phase's name. The open circles connected by the dashed lines represent quadrupolar splitting relative to that of the α -deuteriums, for which an arbitrary value of 100 KHz is taken. The figure shows the characteristic pattern of the quadrupolar splitting along the alkoxy chain.
17. Same as in Figure 16 for 60·7 and 70·7.
18. Bond diagram of an even carbon atom in an all-trans chain. The numbers in parentheses indicate the bond type as discussed in the text. Also given are expressions for the various bond angles relative to the long molecular axis, L, assuming \angle CCC and \angle DCD to be tetrahedral angles.
19. Calculated relative quadrupole splitting of the alkoxy deuterons as function of position along the chain for 5, 6, 7 and 8 membered alkoxy chains for different values of the angle α' . The α -carbon splitting was arbitrarily set equal to 1.0 and the kink probabilities were assumed to be linear in i according to Eq. (VI.5). Note that the sign of Δ for the methyl deuterons in 50·7 and 70·7 is opposite to that of the Δ -methylene deuterons while all other Δ 's have the same sign.

20. Orientation relative to L, of the end methyl groups in the all-trans conformation of odd- and even-membered chains.
21. Same as in Figure 19 for an hexyloxy chain in which both α' and P^2 are varied as indicated. The kink probabilities are assumed to obey the relation $P^i = P^2 + (i-2)0.06$ ($i \geq 2$).
22. Calculated kink probabilities in 40.7 and 50.7 for selected temperatures (one for each mesophase). For the calculations the methylene quadrupole splittings of Figure 16 were used with $\alpha' = 20^\circ$ and $P^2 = 0.05$. The open symbols were calculated from the methyl resonance.
23. Same as Figure 22 for 60.7 and 70.7 using the data of Figure 17, $\alpha' = 20^\circ$ and $P^2 = 0.01$.
24. Stick diagrams of NMR spectra of spin $I = 1$ nuclei for the three cases discussed in Appendix A. (a) Two inequivalent nuclei with $\nu_Q^B > \nu_Q^A > 0$ and $|D| \ll |\nu_Q^A + \nu_Q^B|$. (b) Three equivalent nuclei with D_3 permutation symmetry and $|D| \ll |\nu_Q|$. (c) The case $AA'B$ with $|D^{AA'}| \ll |\nu_Q^A|$, $|D^{AB}|$, $|D^{A'B}| \ll |\nu_Q^A - \nu_Q^B|$, and using $SD/D = 0.62$ and $RD/D = 0.15$. The transians of order $\sin^2 2\alpha$ and splittings of order Δ are too small to observe on the scale of the figure. For cases a and b two spectra for the two possible relative signs of D and ν_Q are given.



XBL778-5960

Figure 1

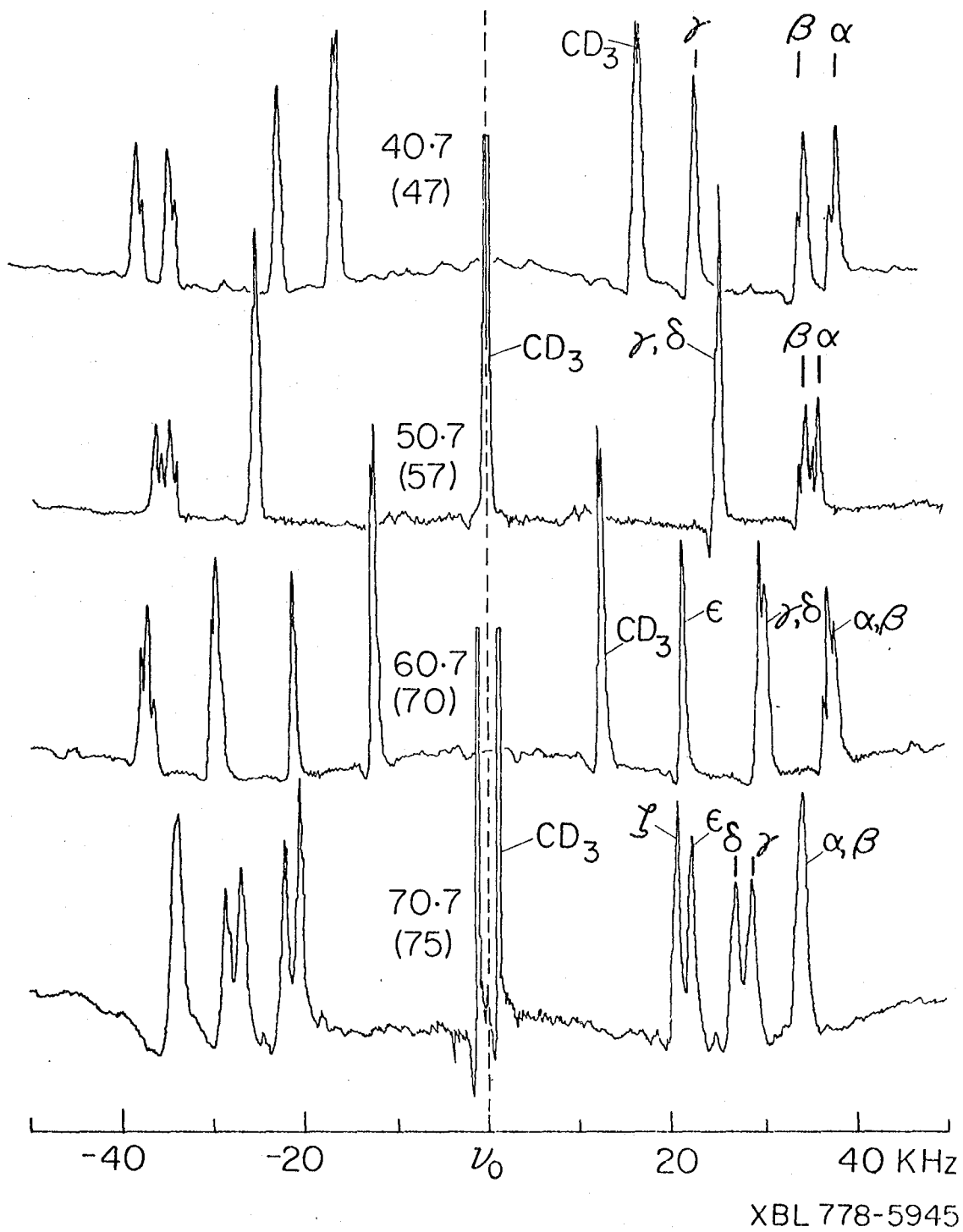
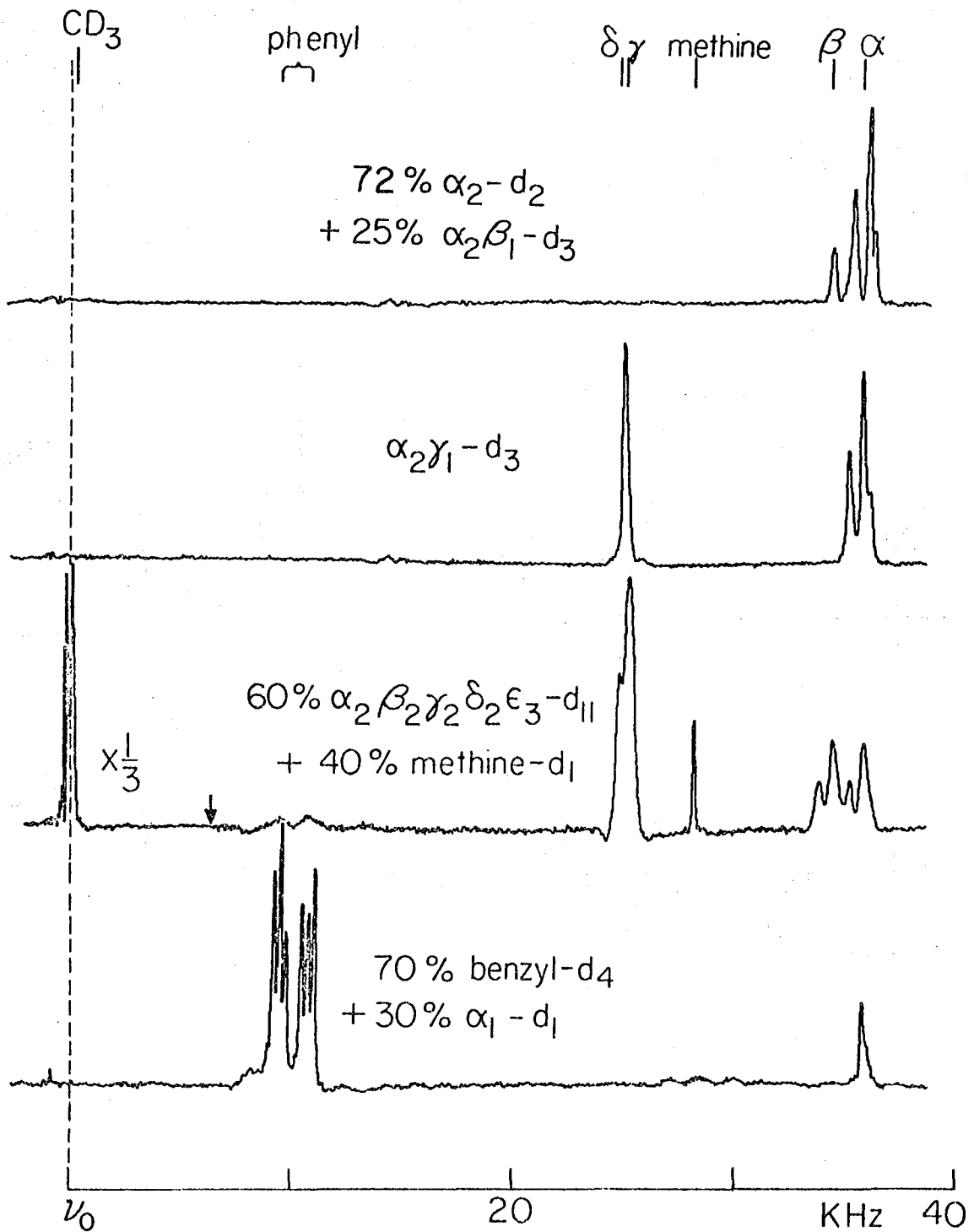
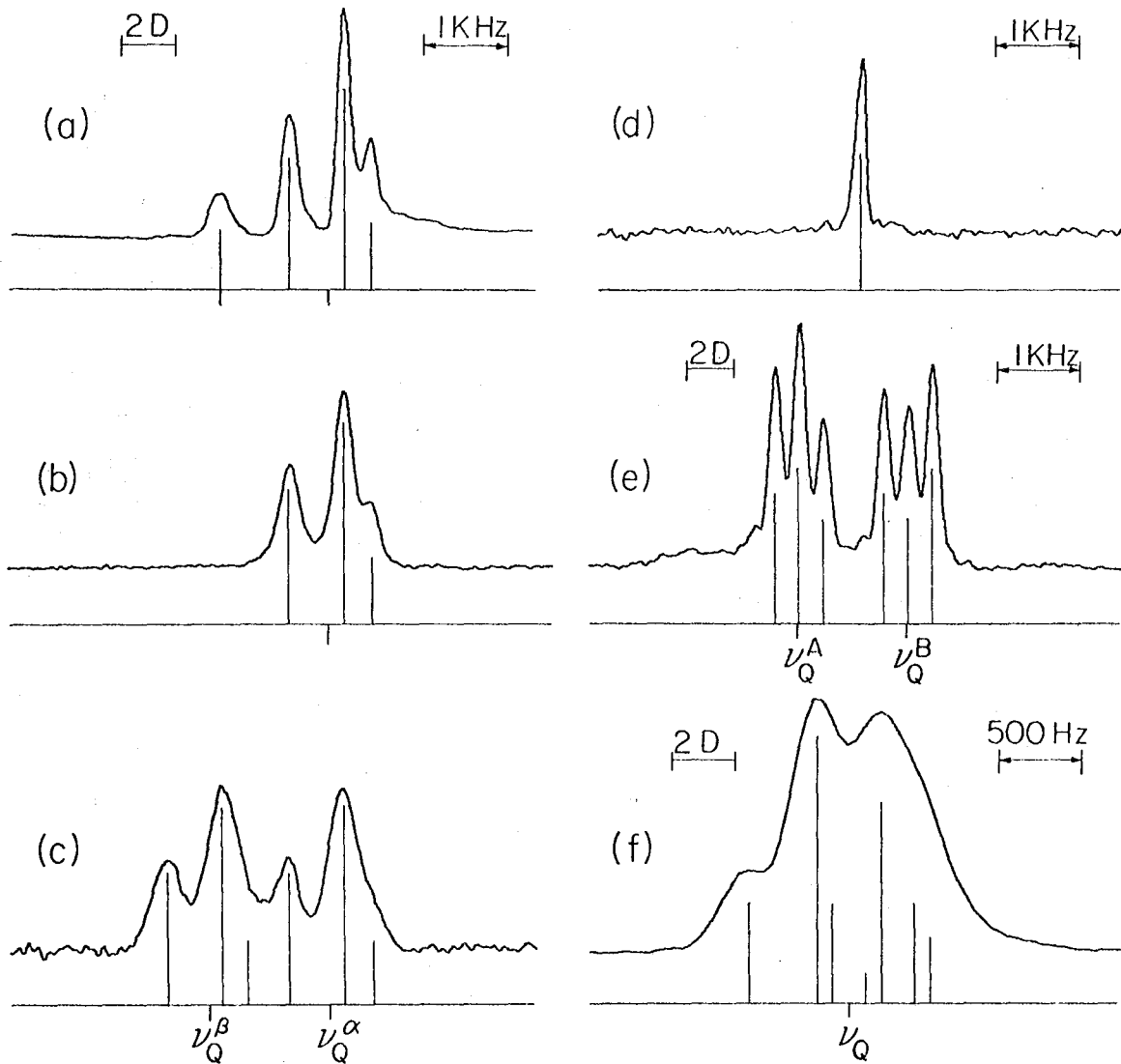


Figure 2



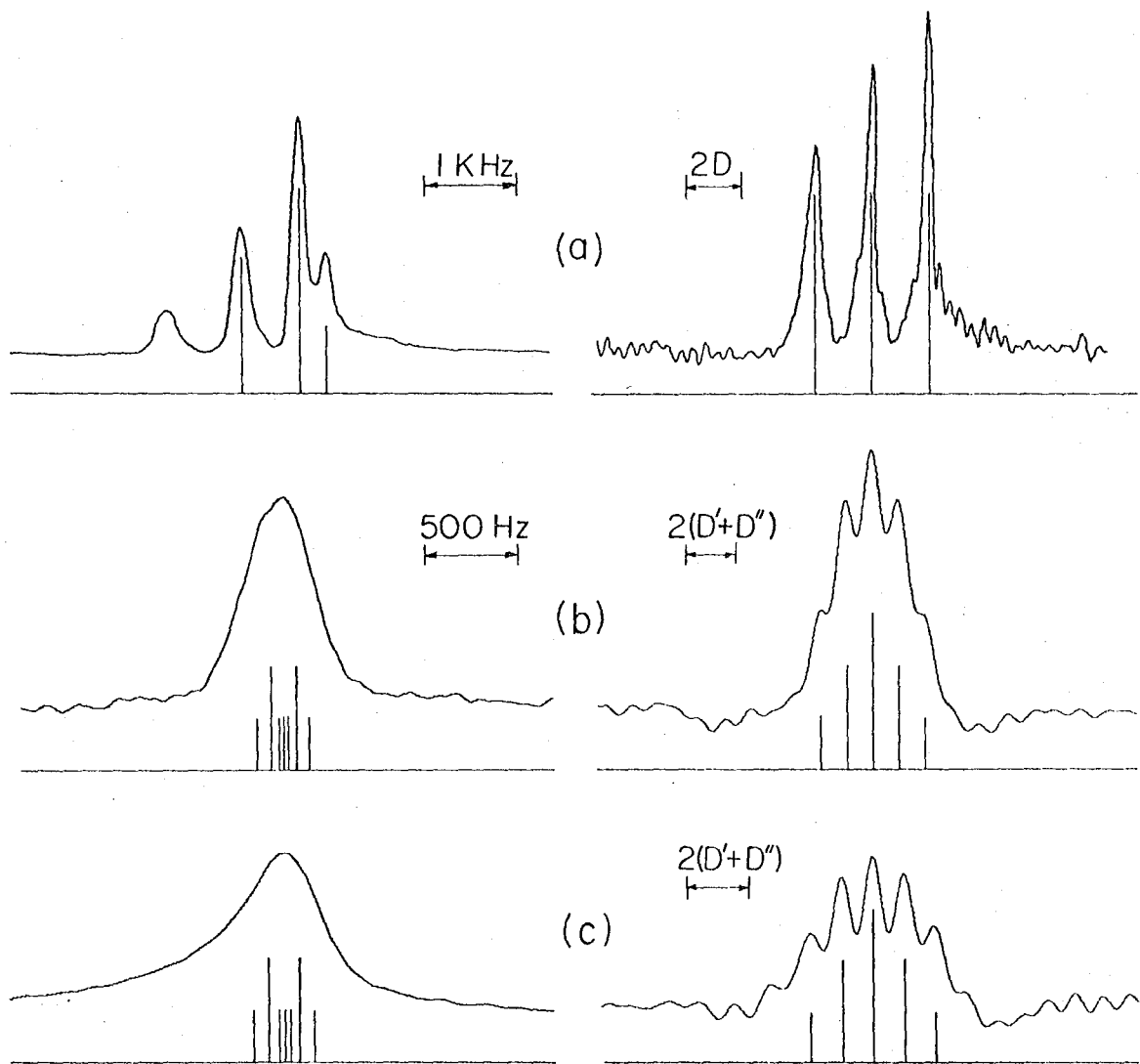
XBL 778-5943

Figure 3



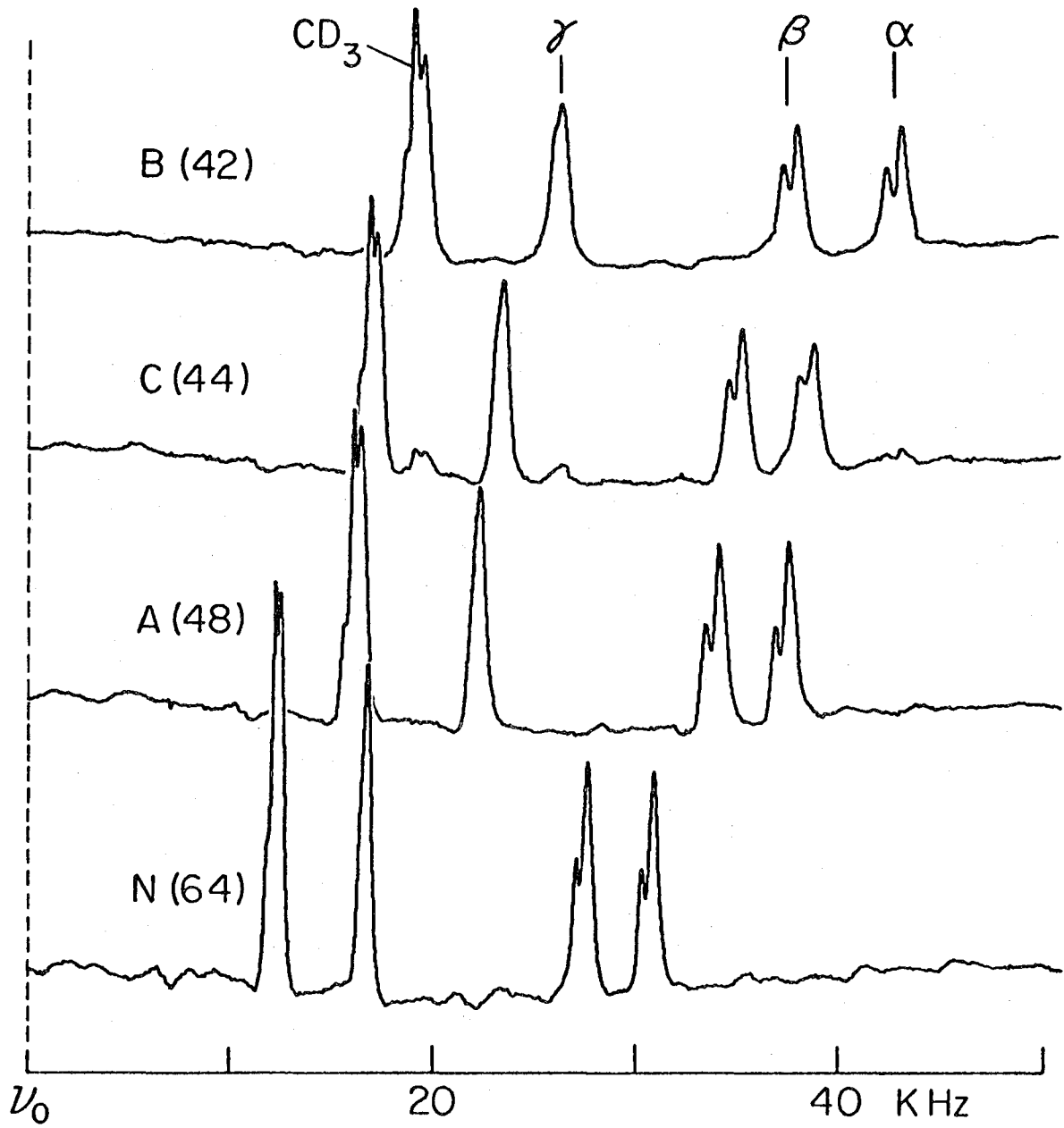
XBL778-5939

Figure 4



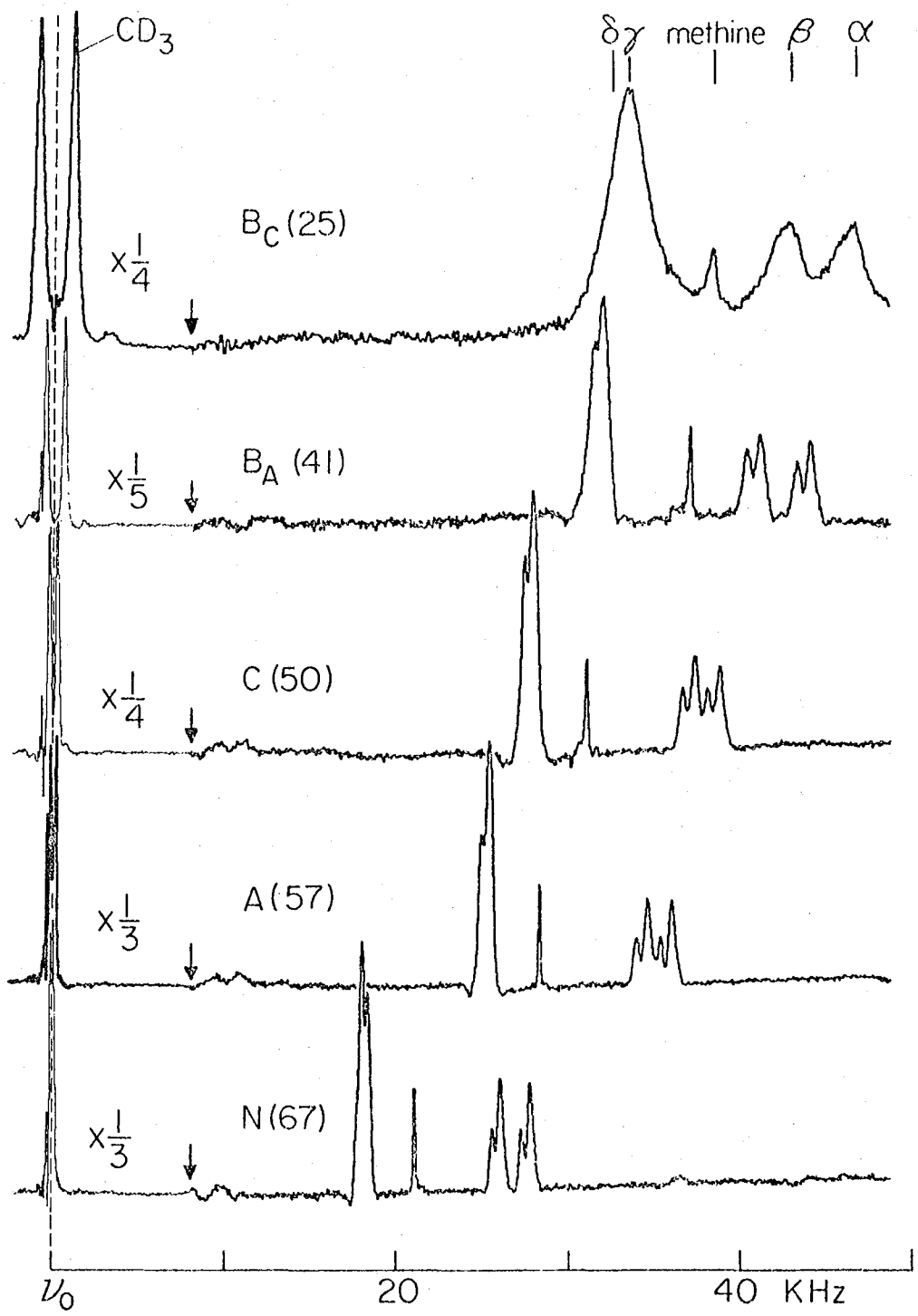
XBL778-5938

Figure 5



XBL 778-5942

Figure 6



XBL778-5941

Figure 7

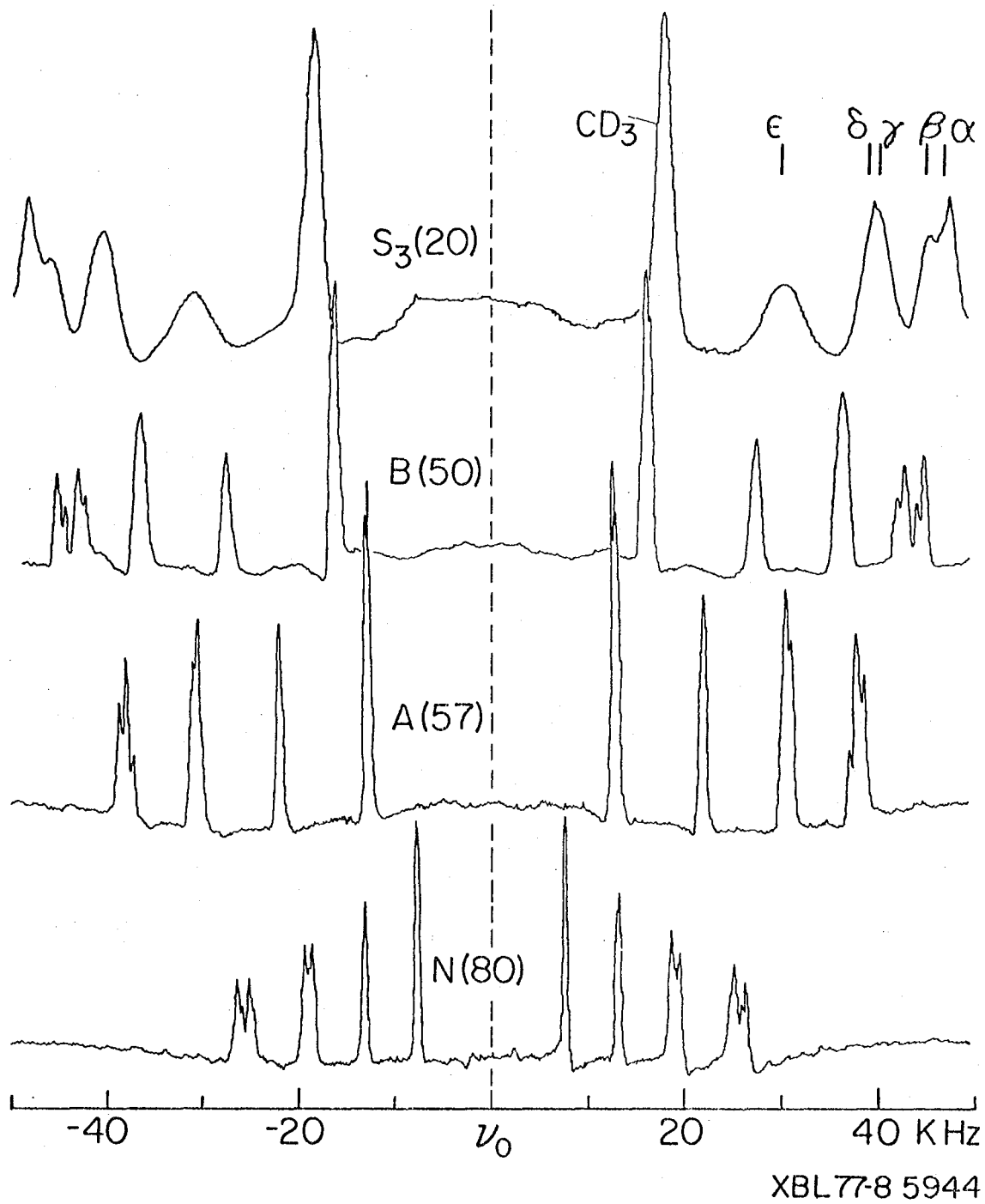
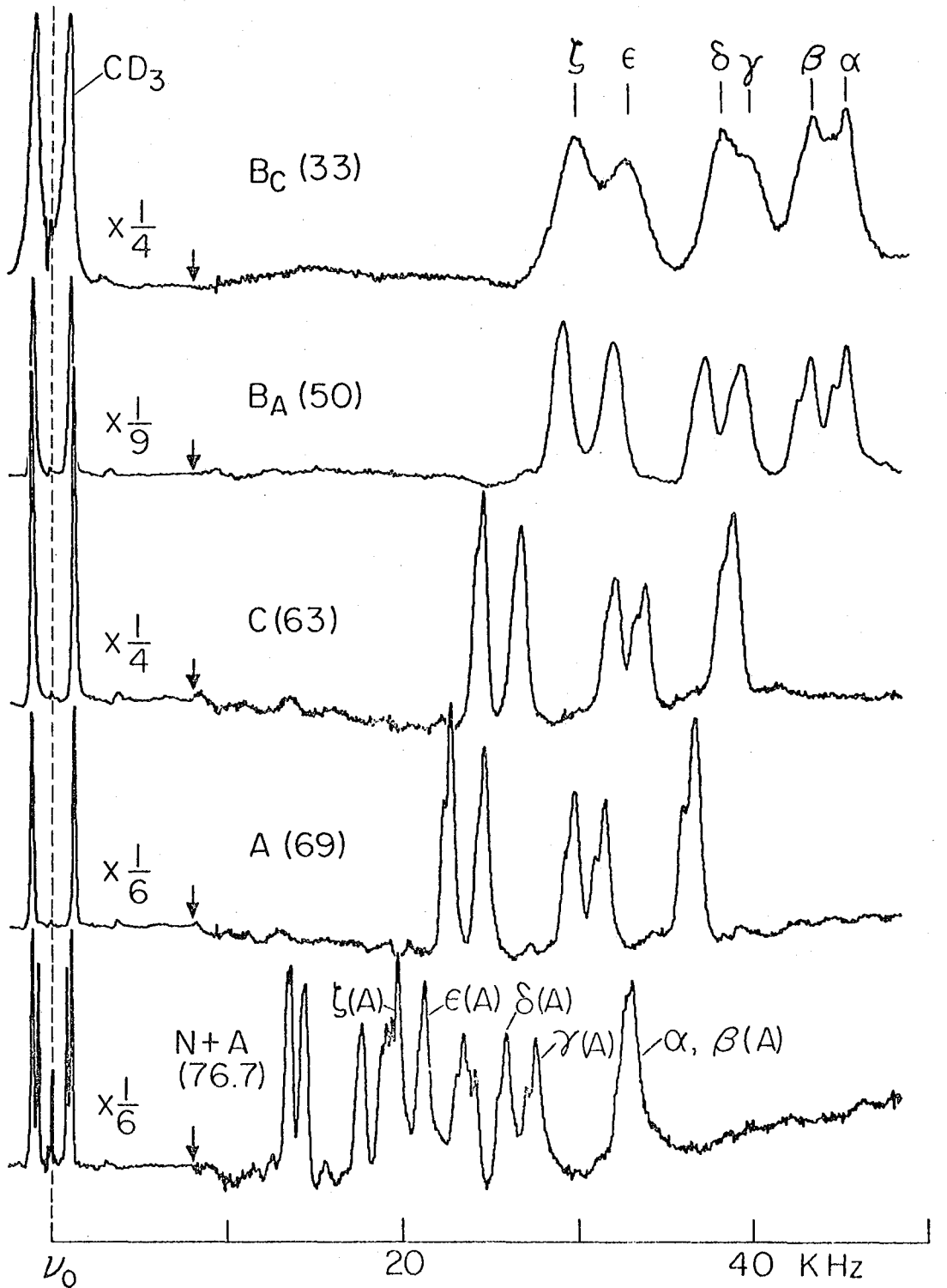
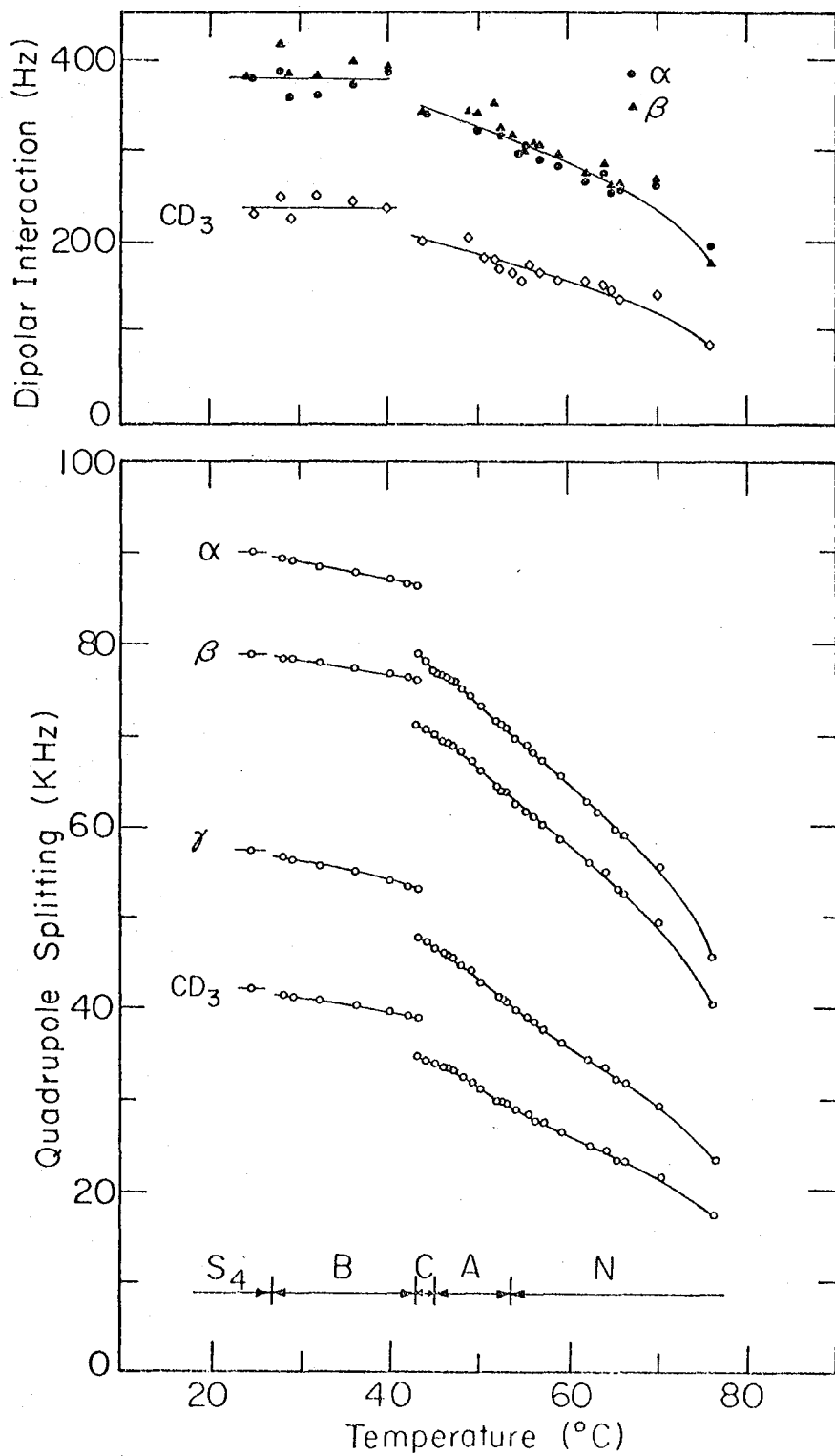


Figure 8



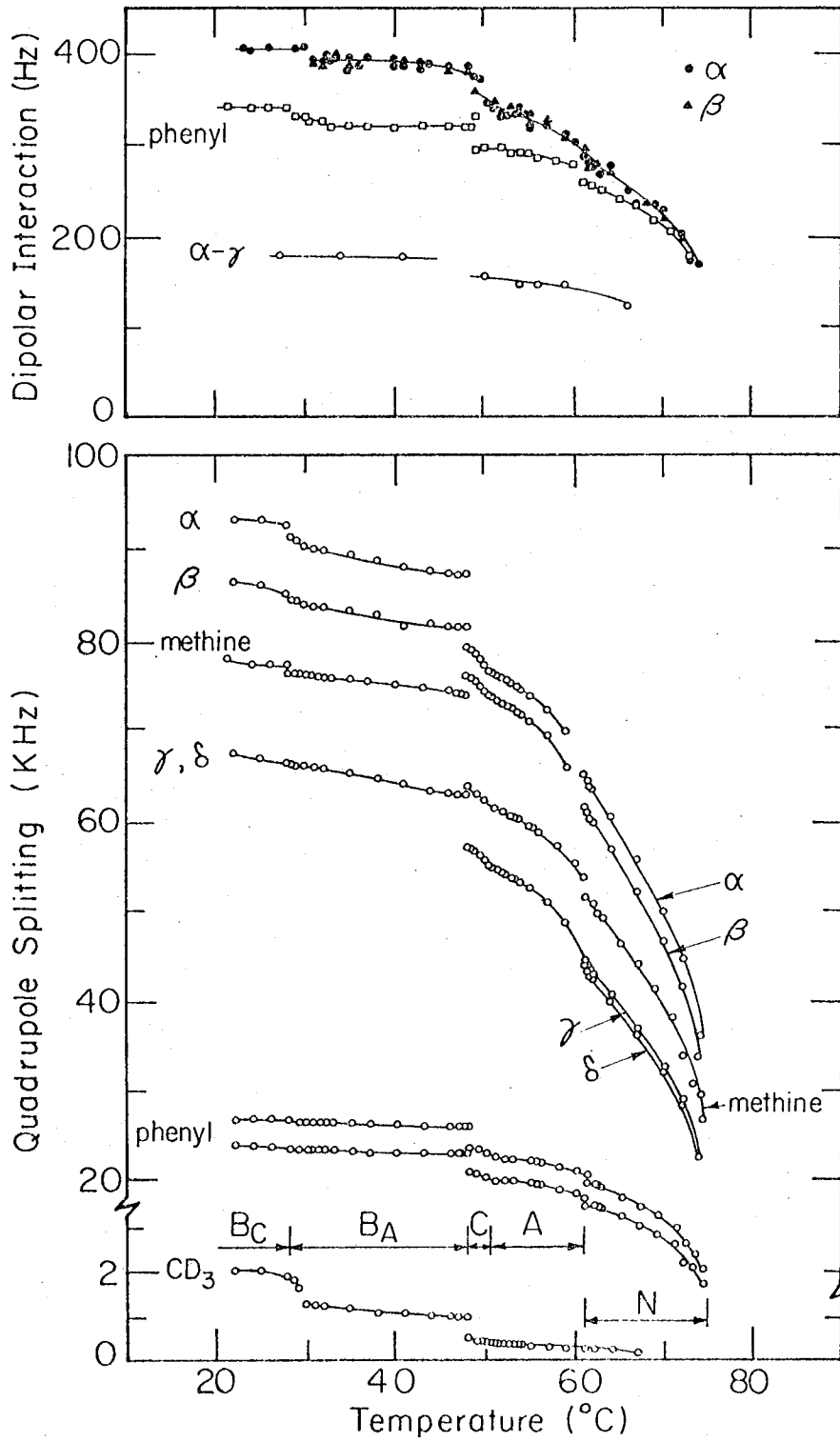
XBL 778-5940

Figure 9



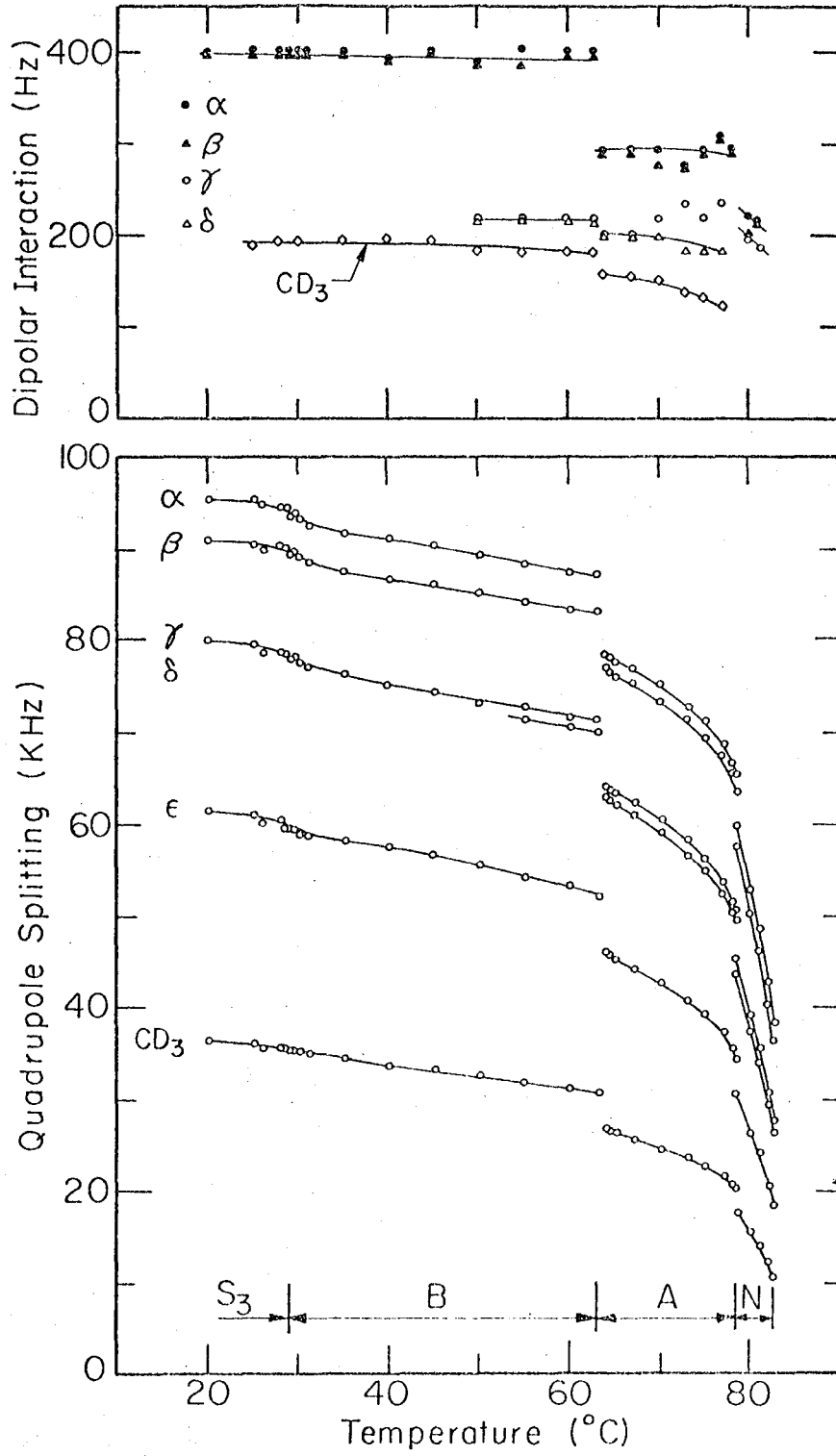
XBL 778-5956

Figure 10



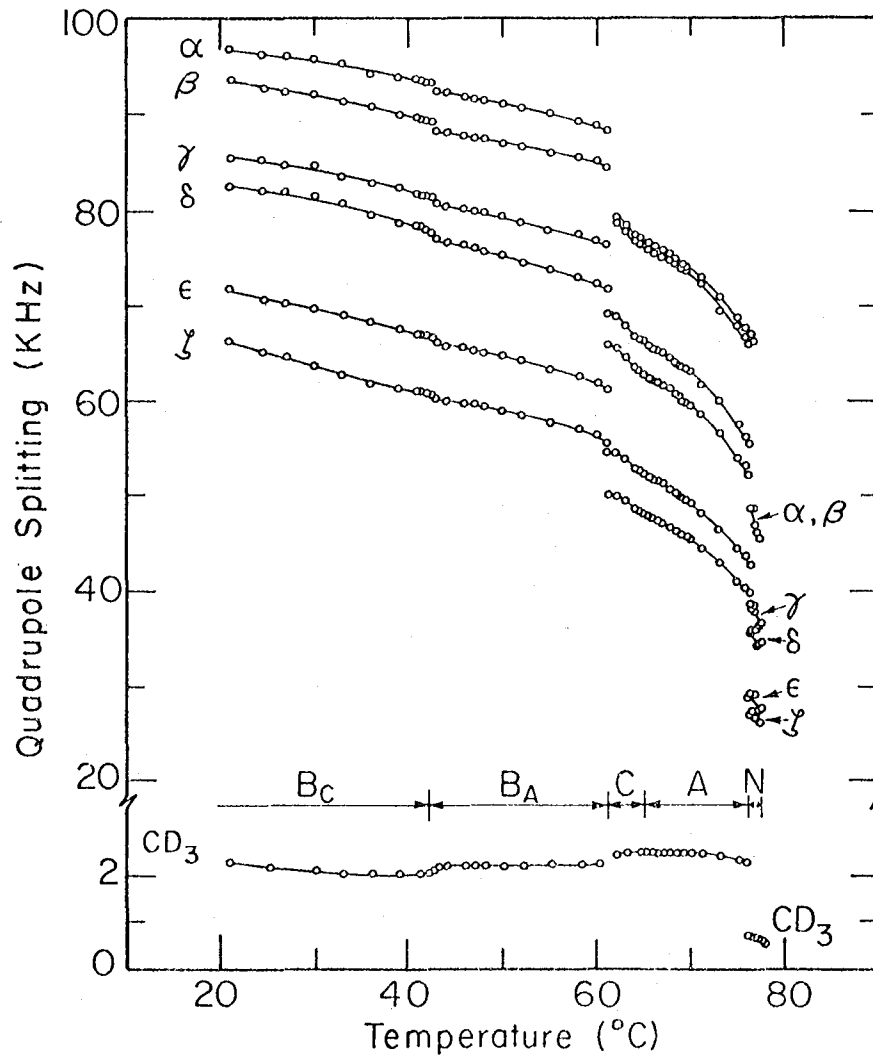
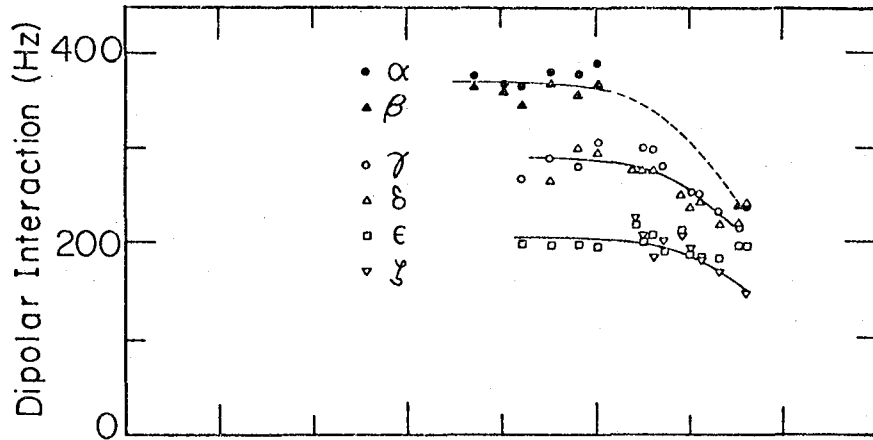
XBL 778-5958

Figure 11



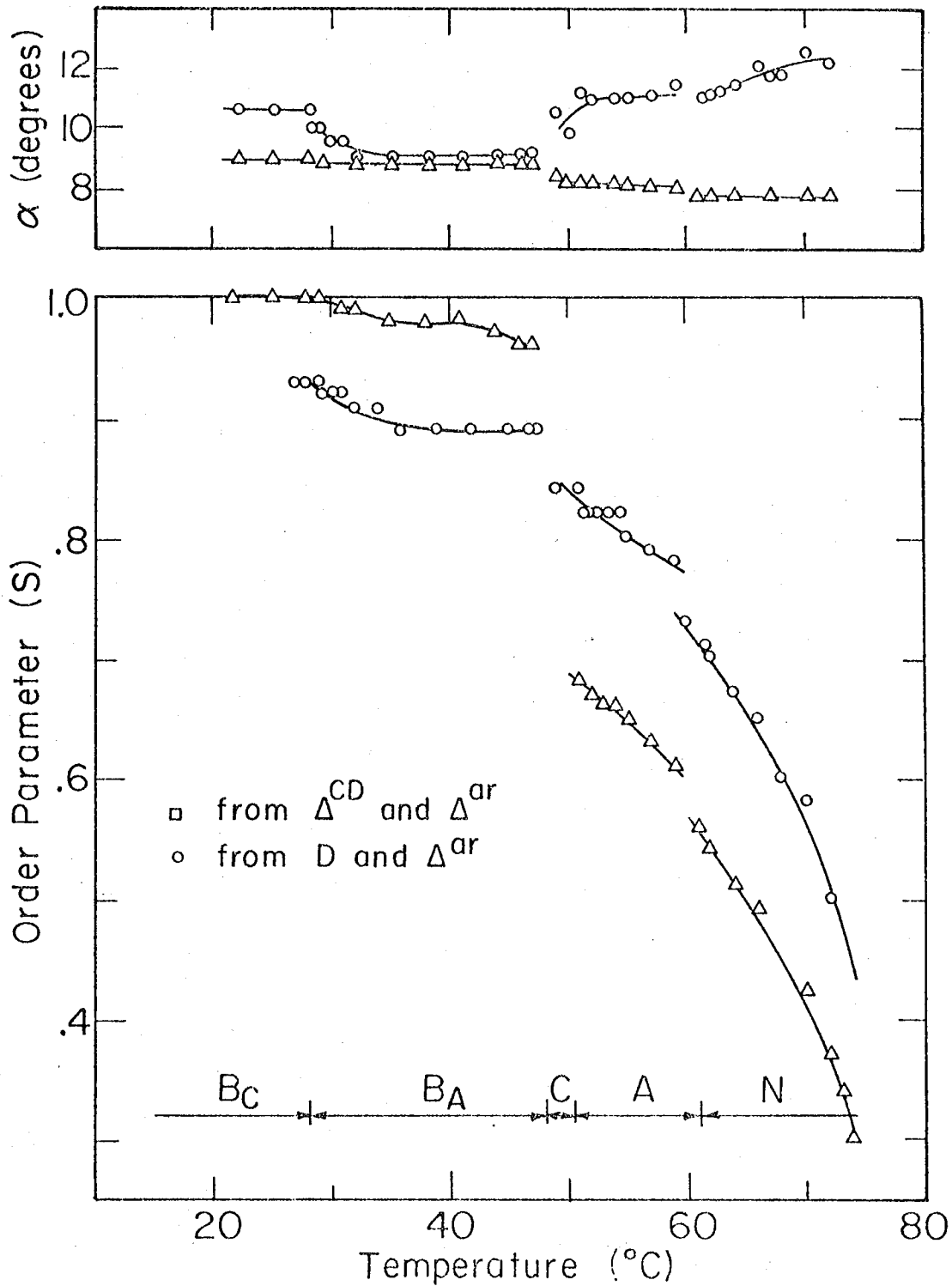
XBL 778-5955

Figure 12



XBL778-5957

Figure 13



XBL 778-6010

Figure 14

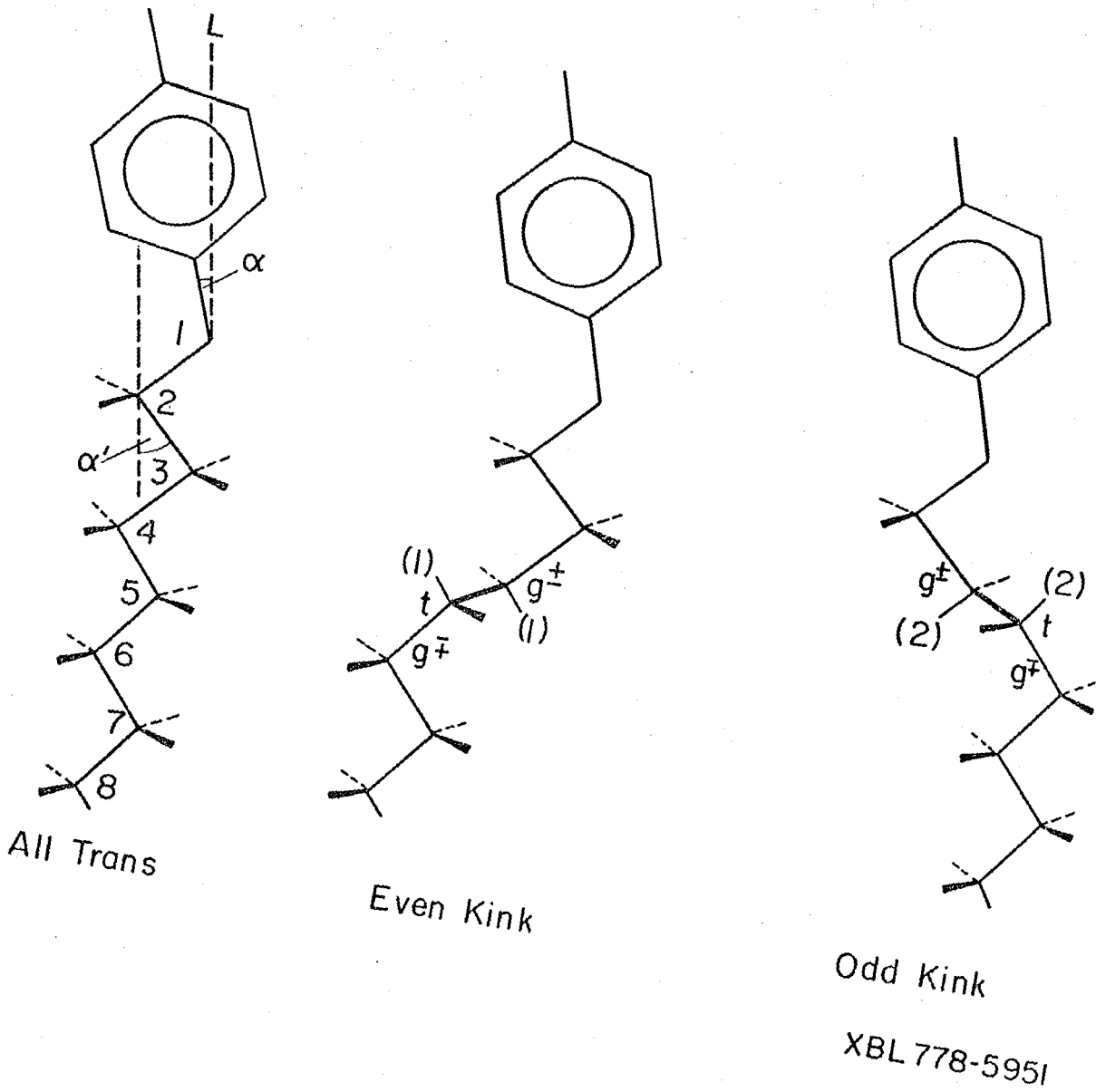
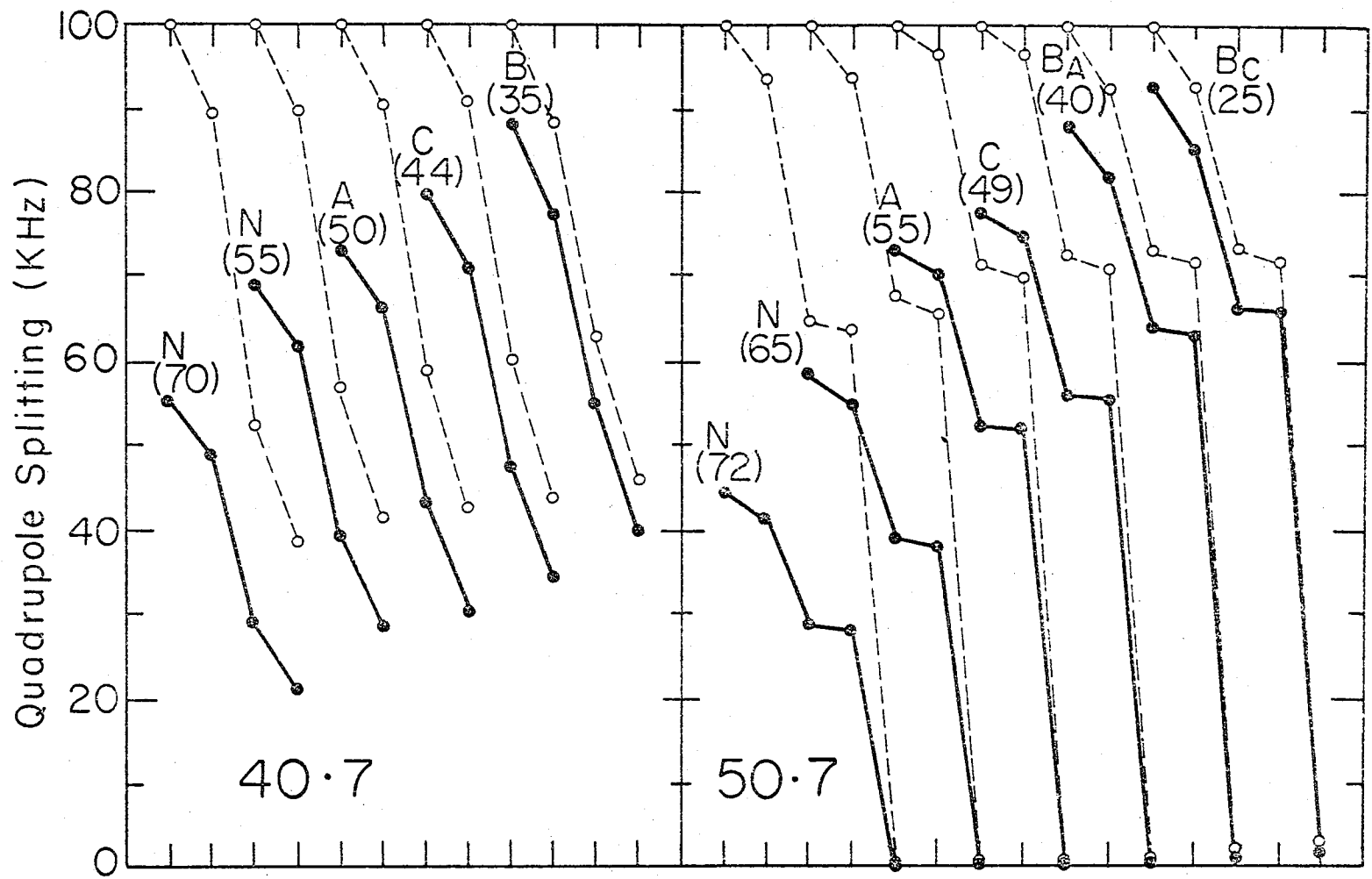
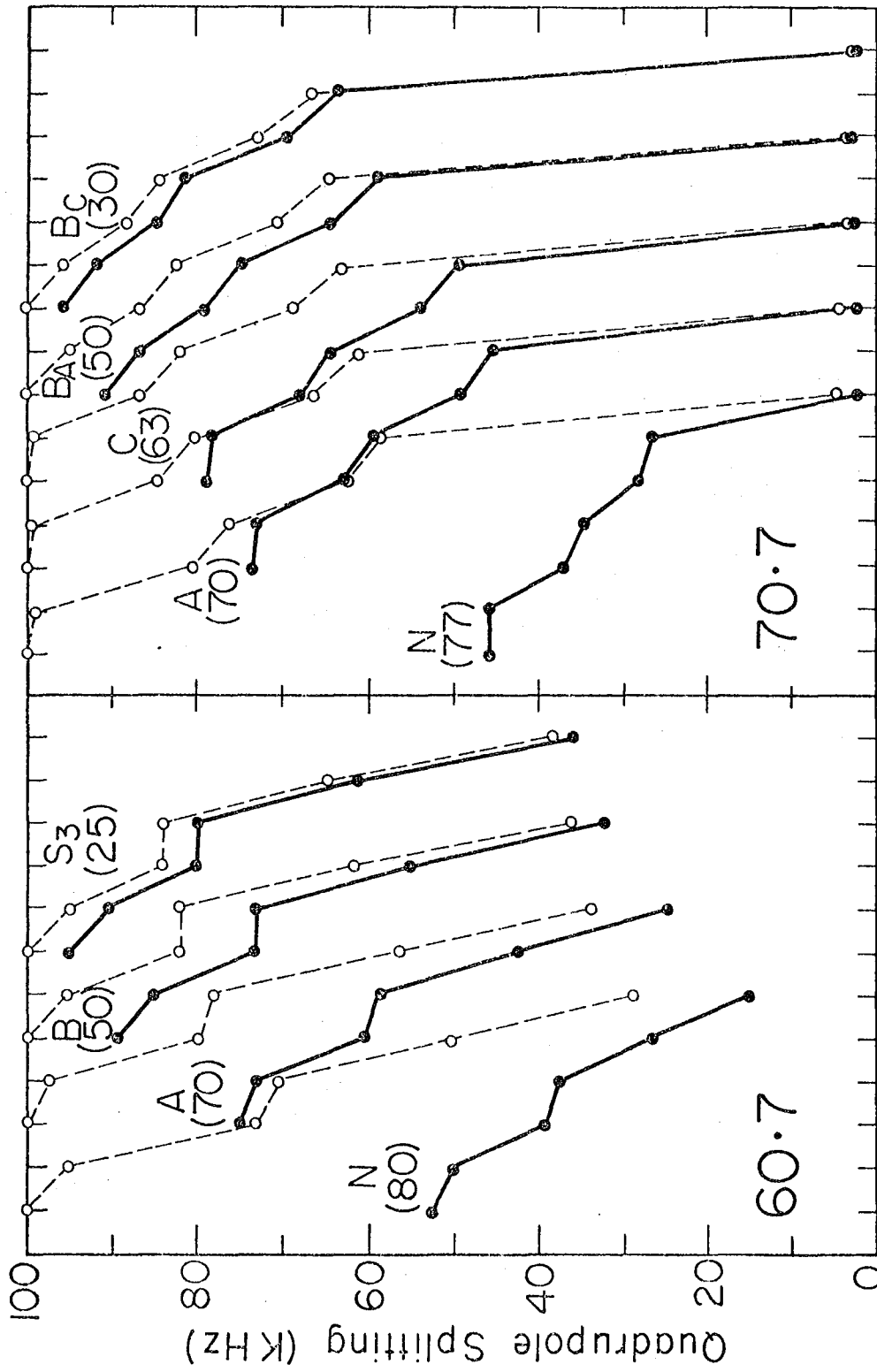


Figure 15



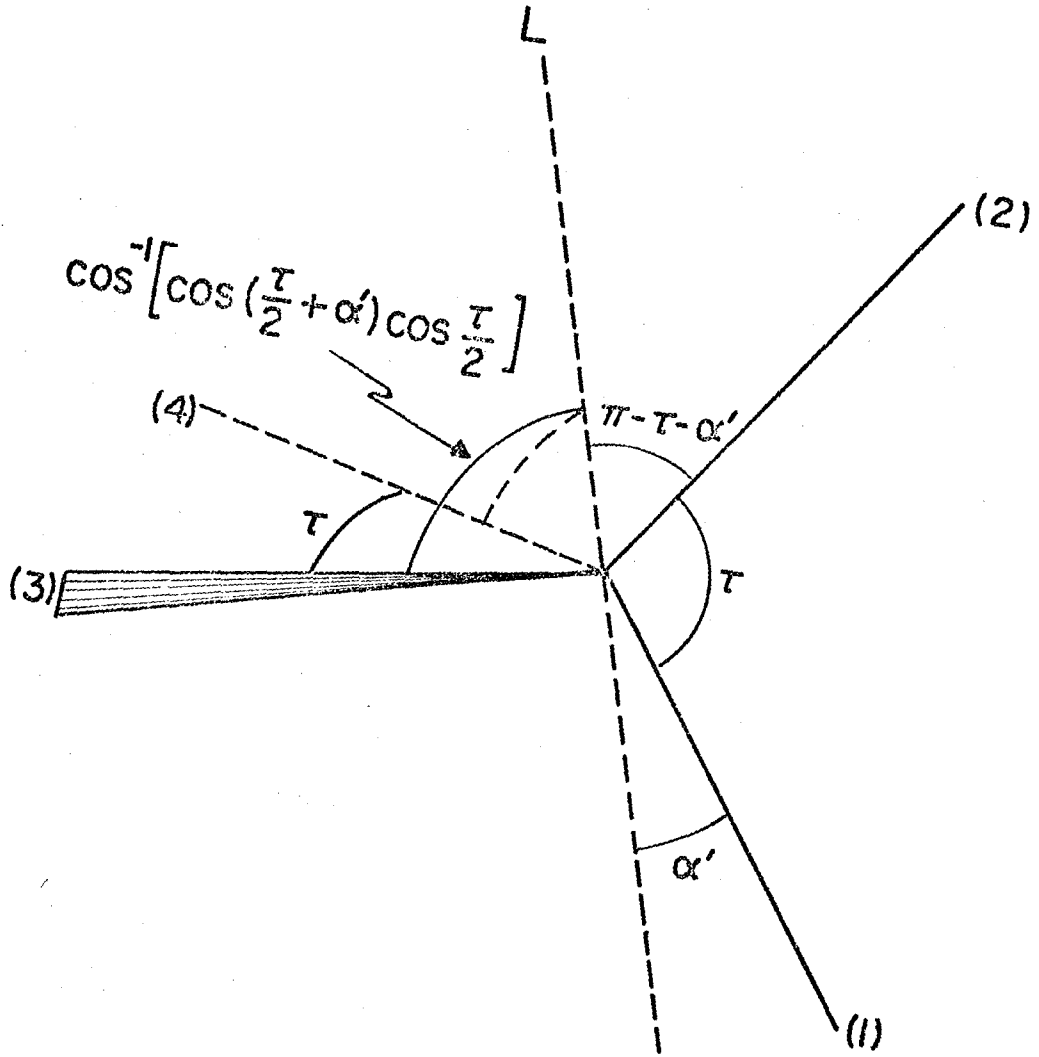
XBL 778-5953

Figure 16



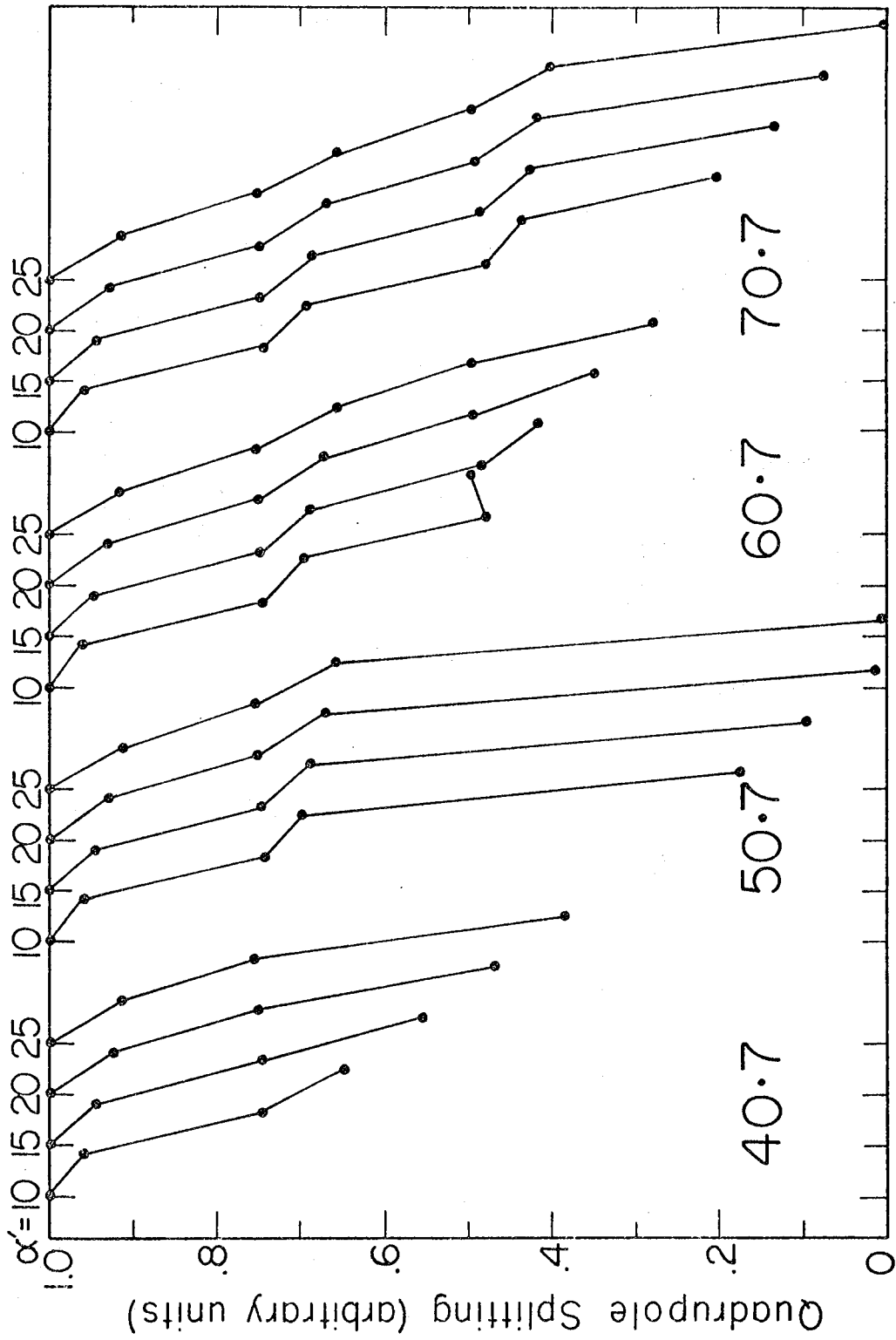
XBL778-5954

Figure 17



XBL 778-5948

Figure 18



XBL 778-5959

Figure 19

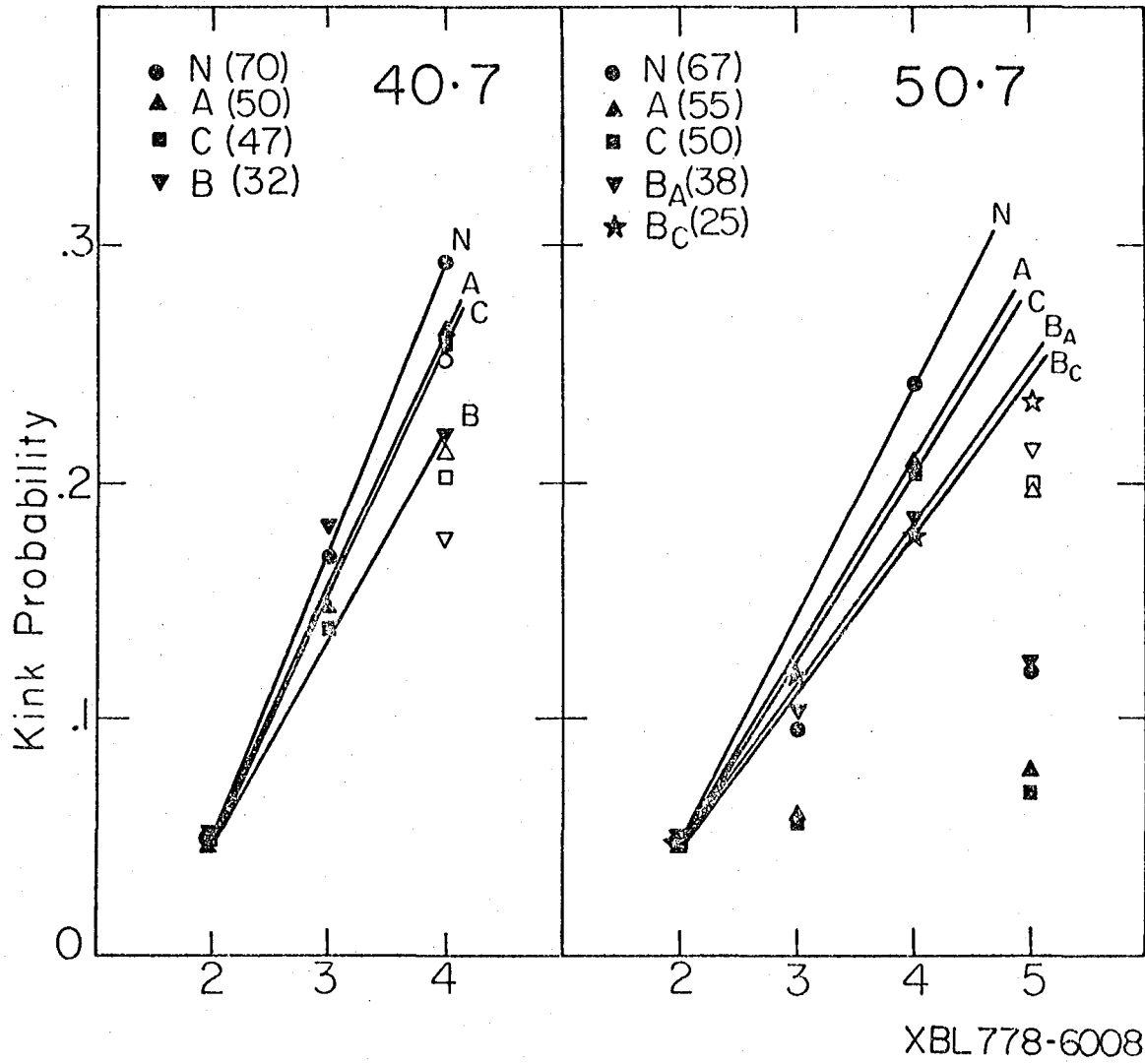
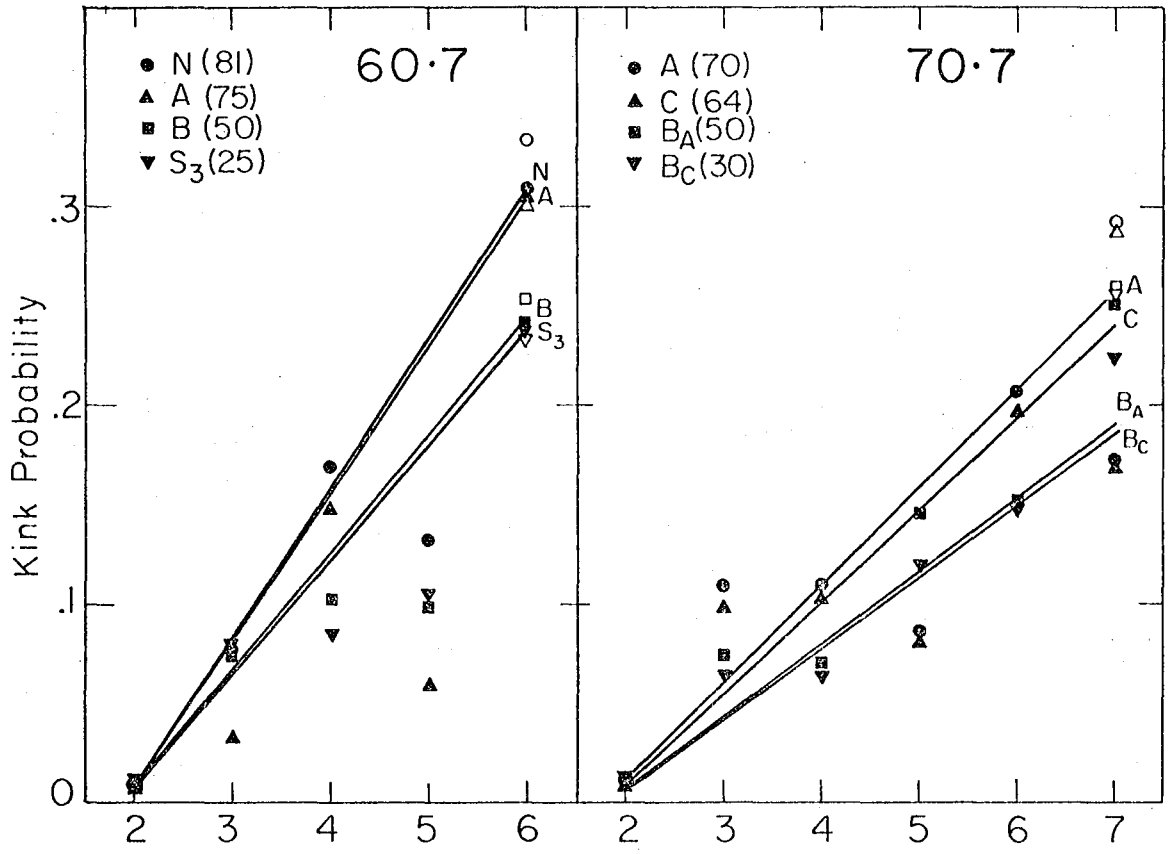


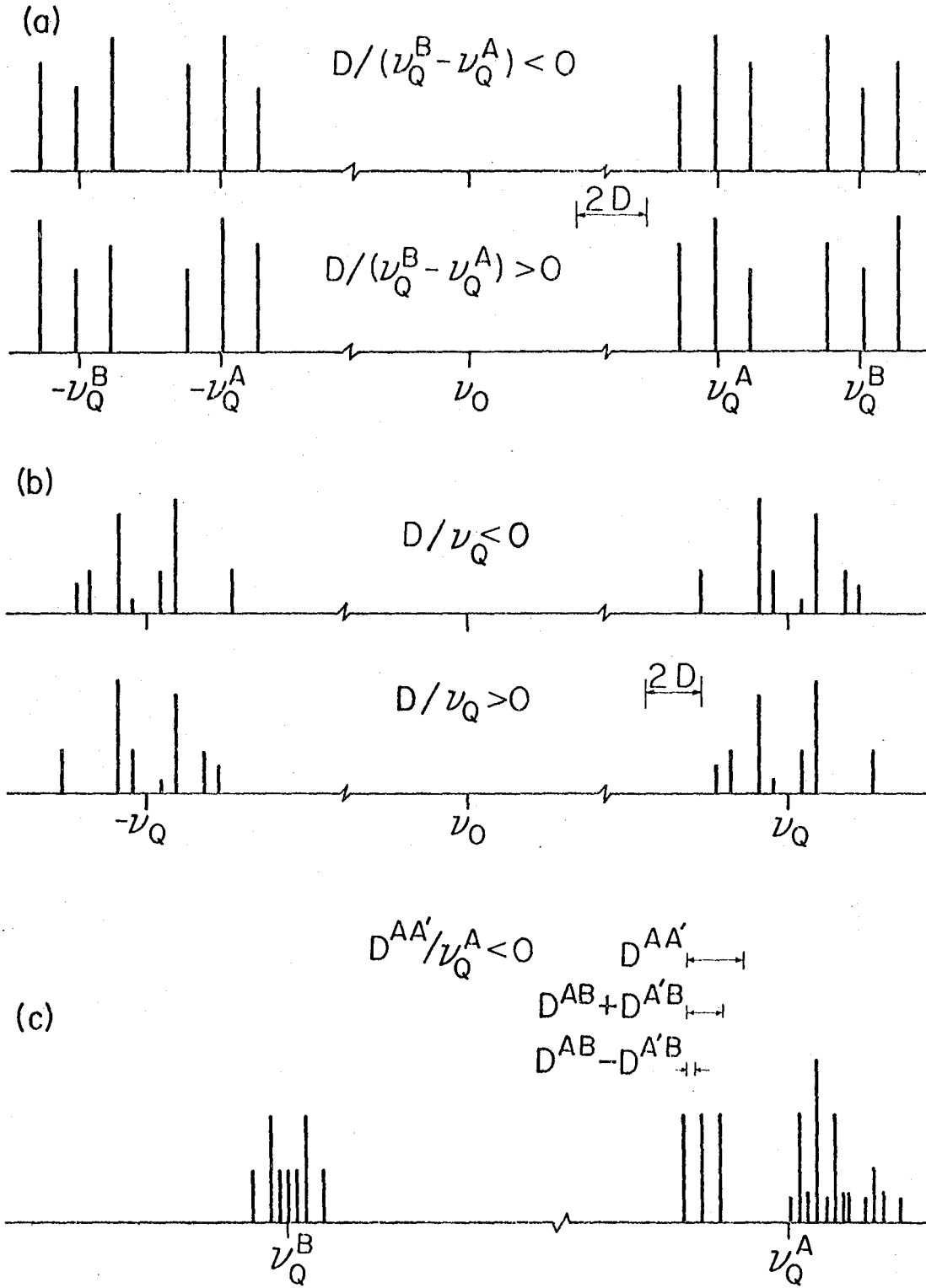
Figure 22

XBL 778-6008



XBL 778-6009

Figure 23



XBL 778-5952

Figure 24

This report was done with support from the United States Energy Research and Development Administration. Any conclusions or opinions expressed in this report represent solely those of the author(s) and not necessarily those of The Regents of the University of California, the Lawrence Berkeley Laboratory or the United States Energy Research and Development Administration.